Integrated Direct/Indirect Adaptive Robust Posture Trajectory Tracking Control of a Parallel Manipulator Driven by Pneumatic Muscles

Xiaocong Zhu, Guoliang Tao, Bin Yao, *Member, IEEE*, and Jian Cao

***Abstract*—An integrated direct/indirect adaptive robust controller (DIARC) is proposed to further improve the achievable posture trajectory tracking control performance of a parallel manipulator driven by pneumatic muscles. Due to the model errors of the static forces and friction forces of pneumatic muscles, the simplified average flow rate characteristics of valves, and the unknown disturbances of entire system, there exist large extent of parametric uncertainties and rather severe uncertain nonlinearities in the modeling of the parallel manipulator. To address these problems, in this paper, an indirect type parameter estimation is used to obtain reliable estimates of effective model parameters for reducing the parametric uncertainties while an integrated direct/indirect ARC with dynamic compensation type fast adaptation is utilized to further attenuate the influences of uncertain nonlinearities for better tracking performance. Considering that the conventional parameter estimation algorithm based on single error minimizing criterion normally fails to provide reliable parameter estimation for the parallel manipulator with symmetric structure due to the difficulty in satisfying the persistent exciting conditions all the time—the theoretical requirement for the convergence of online parameter estimation, additional practical constraints are imposed to further condition the parameter estimation process and a new parameter estimation algorithm based on composite error minimizing criterion in task-space is developed. Experimental results demonstrate that the parallel manipulator under the control of the proposed integrated DIARC has strong self-adaptability and robustness with the steady-state posture tracking error being less than 0.01°, average tracking error less than 0.1°, and maximum tracking error less than 0.3°, which are significantly better than those of the direct ARC.**

***Index Terms*—Adaptive control, nonlinear systems, parallel manipulator, parameter estimation, pneumatic muscle.**

I. Introduction

THE pneumatic muscle is a new kind of pneumatic actuator with the advantages of cleanness, lightweight, low cost, easy maintenance, compact structure and high power/volume ratio. It has been gradually applied in industry for on-off control [1]. However, rather severe parametric uncertainties and uncertain nonlinearities exist in the dynamic modeling of pneumatic muscle systems, which posts significant challenges for precise trajectory tracking control. Recently, many researchers have devoted themselves to the investigation on the trajectory tracking control of pneumatic muscle systems [2]–[8]. The parallel manipulator driven by pneumatic muscles (PMDPM) studied in this paper is a new application of pneumatic muscles, which consists of three pneumatic muscles connecting the moving platform of the parallel manipulator to its base platform as shown in Fig. 1. By controlling the lengths of three pneumatic muscles, various rotation motions of the parallel manipulator can be realized. Such a parallel manipulator combines the advantages of compact structure of parallel mechanisms with adjustable stiffness and high power/volume ratio of pneumatic muscles, which will have promising wide applications in robotics, industrial automation, and bionic devices [9], [10].

1.Moving platform 2.Ball joint 3.Spherical joint
4.Pneumatic muscle 5.Central pole 6.Base platform

Fig. 1. Experimental setup of parallel manipulator driven by pneumatic muscles.

Due to the model errors of the static forces and friction forces of pneumatic muscles, the simplified average flow rate characteristics of valves, and the unknown disturbances of entire system, there exist large parametric uncertainties and rather severe uncertain nonlinearities in the modeling of the PMDPM. To address these problems, a direct adaptive robust controller

Manuscript received April 03, 2007; revised January 14, 2008. Manuscript received in final form June 05, 2008. First published February 27, 2009; current version published April 24, 2009. Recommended by Associate Editor C.-Y. Su. This work was supported by National Natural Science Foundation of China under Contract 50775200. The work of B. Yao was supported by the National Natural Science Foundation of China (NSFC) under the Joint Research Fund Grant 50528505 for Overseas Chinese Young Scholars and a Kuang-piu Professorship from Zhejiang University.

The authors are with the State Key Laboratory of Fluid Power Transmission and Control, Zhejiang University, Hangzhou 310027, China (e-mail: zhuxiaoc@zju.edu.cn; gltao@zju.edu.cn; byao@purdue.edu; caojianjiaowang@sina.com.cn).

Color versions of one or more of the figures in this paper are available online at http://ieeexplore.ieee.org.

Digital Object Identifier 10.1109/TCST.2008.2001715

(DARC) has been developed to reduce the large extent of lumped uncertain nonlinearities and parametric uncertainties while using certain robust feedback to attenuate the influences of uncompensated uncertain nonlinearities [11]–[13]. However, the DARC, which only utilizes the parameter adaptation based on tracking error dynamics to compensate the large model errors associated with pneumatic muscle system, cannot tackle the fast-varying model errors in the process of posture trajectory control, resulting in not so satisfying transient tracking errors. To further improve achievable posture trajectory tracking accuracy, it is necessary to construct a parametric model for the lumped uncertain nonlinearities and compensate these uncertainties by parameter adaptation. When these parametric models are used in the DARC, it is typically difficult to determine the suitable adaptation rate since the estimation algorithms in the DARC are of gradient type and there are too many unknown parameters to be adapted. It is observed through experiments that when the adaptation rate matrix is inappropriately chosen, large tracking errors and even vibrations of the PMDPM will occur. To overcome these practical problems of the DARC, in this paper, an indirect type parameter estimation is used to obtain reliable estimates of effective model parameters for reducing the parametric uncertainties while an integrated direct/indirect ARC [14] with dynamic compensation type fast adaptation is utilized to further attenuate the influences of uncertain nonlinearities for better tracking performance. But yet, for the posture trajectory tracking control of the PMDPM with redundancy, when the conventional parameter estimation algorithm based on single error minimizing criterion in task-space is used, the experimental results of the proposed integrated DIARC is not so satisfactory as expected. A closer look at the problem reveals that it is typically difficult to satisfy the persistent exciting conditions all the time, which are required for the convergence of online parameter estimation. As a result, unreliable and inaccurate parameter estimates with large covariance may appear when the conventional parameter estimation algorithm is used [15], [16]. To bypass this difficulty, in this paper, additional practical constraints are imposed to further condition the parameter estimation process and a new parameter estimation algorithm based on composite error minimizing criterion in task-space is developed.

This paper is organized as follows. The dynamic models of the PMDPM controlled by fast switching valves are presented in Section II. The proposed parameter estimation algorithms for the parallel manipulator dynamics and the actuator dynamics are given in Section III. An integrated direct/indirect adaptive robust controller (DIARC) is synthesized for the system in Section IV, along with stability proofs for the resulting closed-loop system. Experimental results are shown in Section V to verify the effectiveness of the proposed integrated DIARC, and conclusions are drawn in Section VI.

II. Dynamic Models

The PMDPM is shown in Fig. 1, which consists of a moving platform, a base platform, a central pole and three pneumatic muscles connected by six ball joints that are evenly distributed along the respective platforms. The central pole is fixed to the base platform and is connected to the moving platform by a spherical joint. The reference frame is fixed to the base platform and the moving frame is attached to the moving platform at the center. The posture of the PMDPM is defined through the standard roll-pitch-yaw (RPY) angles: first rotate the moving frame around the fixed x-axis by the yaw angle θ_x, then rotate the moving frame around the fixed y-axis by the pitch angle θ_y, and finally rotate the moving frame around the fixed z-axis by the roll angle θ_z. Two fast switching valves (MHE2-MS1H-3/2G-M7-K by Festo) are utilized to control the pressure inside a pneumatic muscle (MAS-40-N600-AA-MCKK by Festo), which is later referred to as a driving unit. Three pressure transducers (SDE-10-10V/20mA by Festo) and position transducers (WS31–250-R1K-L35–1 by ASM) are used to measure the pressures and the contractive lengths of pneumatic muscles respectively. The posture of the PMDPM is then calculated based on the measurement of the lengths of all the three pneumatic muscles. Further information on the experimental setup can be found in [9].

A. Dynamics of Parallel Manipulator

Due to the symmetric placement of three pneumatic muscles in the parallel manipulator studied in the paper, the rotation around z-axis is close to zero ($\theta_z \approx 0^\circ$) and not of practical interests for our applications. Thus, θ_z will be neglected and not controlled, i.e., the parallel manipulator will be considered as having a two-degrees-of-freedom rotation in task-space with one redundant actuation. With these considerations, dynamics of the parallel manipulator in task-space can be described by [13]

$$\boldsymbol{M}(\boldsymbol{\theta})\ddot{\boldsymbol{\theta}}+\boldsymbol{C}(\boldsymbol{\theta},\dot{\boldsymbol{\theta}})\dot{\boldsymbol{\theta}}+\boldsymbol{G}(\boldsymbol{\theta})+\boldsymbol{d}_t(t)=\boldsymbol{J}^{\mathrm{T}}(\boldsymbol{\theta})\boldsymbol{F}_m(\boldsymbol{x}_m,\dot{\boldsymbol{x}}_m,\boldsymbol{p}) \quad (1)$$

where $\boldsymbol{\theta}=[\theta_x,\theta_y]^{\mathrm{T}}$ is the posture vector of the parallel manipulator, $\boldsymbol{x}_m=[x_{m1},x_{m2},x_{m3}]^{\mathrm{T}}$ is the contractive length vector of three pneumatic muscles, $\boldsymbol{p}=[p_1,p_2,p_3]^{\mathrm{T}}$ is the pressure vector inside pneumatic muscles, $\boldsymbol{M}(\boldsymbol{\theta})$ is the rotational inertial matrix, $\boldsymbol{C}(\boldsymbol{\theta},\dot{\boldsymbol{\theta}})\dot{\boldsymbol{\theta}}$ is the vector of centripetal and Coriolis torques, $\boldsymbol{G}(\boldsymbol{\theta})$ is the vector of gravitational torques, $\boldsymbol{d}_t(t)$ is the disturbance vector in task-space, $\boldsymbol{J}(\boldsymbol{\theta})$ is the Jacobian transformation matrix, and $\boldsymbol{F}_m=[F_{m1},F_{m2},F_{m3}]^{\mathrm{T}}$ is the contractive force vector of three pneumatic muscles. Using virtual work principle, several models of the pneumatic muscle's contractive force have been developed [17]–[21]. Such theoretical contractive force is usually inaccurate, which will produce large tracking errors in the posture trajectory tracking control of the PMDPM. Therefore, to improve control accuracy, each component of $\boldsymbol{F}_m$ is expressed as the following parametric form:

$$\begin{aligned}
&F_{mi}(x_{mi},\dot{x}_{mi},p_i)\\
&\quad=F_{m0i}(x_{mi},p_i)-F_{mf0i}(x_{mi},\dot{x}_{mi},p_i)\\
&\qquad+\Delta F_{m0i}(x_{mi},p_i)-\Delta F_{mfi}(x_{mi},\dot{x}_{mi},p_i) \quad (2)\\
&\Delta F_{m0i}(x_{mi},p_i)\\
&\quad=\Delta A_i(x_{mi})p_i+\Delta F_{ri}(x_{mi})\\
&\quad=(a_0+a_1x_{mi}+a_2x_{mi}^2+a_3x_{mi}^3)p_i\\
&\qquad+\left(b_0+b_1x_{mi}+b_2x_{mi}^2+b_3x_{mi}^3\right) \quad (3)
\end{aligned}$$

$$\begin{aligned}&\Delta F_{mfi}(x_{mi},\dot{x}_{mi},p_i)\\&\quad=\left[\left(a_{f0}+a_{f1}x_{mi}+a_{f2}x_{mi}^2+a_{f3}x_{mi}^3\right)p_i\right.\\&\qquad\left.+\left(b_{f0}+b_{f1}x_{mi}+b_{f2}x_{mi}^2+b_{f3}x_{mi}^3\right)\right]\operatorname{sign}(\dot{x}_{mi})\end{aligned}\tag{4}$$

where F_{m0i} and F_{mf0i} ($i = 1, 2, 3$) are the theoretical static force model and friction force model of pneumatic muscle used in the previous literature respectively, in which F_{m0i} can be written as $F_{m0i}(x_{mi},p_i) = A_i(x_{mi})p_i + F_{ri}(x_{mi})$ by neglecting certain complex terms [19]. ΔF_{m0i} and ΔF_{mfi} represent the static force and friction force of pneumatic muscles that are not captured by the traditional models F_{m0i} and F_{mf0i}, respectively. ΔF_{m0i} and ΔF_{mfi} are further parameterized by the models in (3) and (4), respectively, in which ΔA_i and ΔF_{ri} represent the pressure gain and the pressure independent terms in ΔF_{m0i}, respectively, a_0, a_1, a_2, a_3, b_0, b_1, b_2, and b_3 are the parameters used for ΔF_{m0i}, and a_{f0}, a_{f1}, a_{f2}, a_{f3}, b_{f0}, b_{f1}, b_{f2}, and b_{f3} are the parameters for ΔF_{mfi}. Since the pneumatic muscles used in this paper are identical, for simplicity, the same parameters are assumed for all the three pneumatic muscles. The small amount of parameter variations among various pneumatic muscles can be lumped into the uncertain nonlinearities and attenuated by robust feedback later.

Through combining (1) and (2)–(4), the dynamics of the parallel manipulator can be rewritten as

$$\begin{aligned}&\boldsymbol{M}(\boldsymbol{\theta})\ddot{\boldsymbol{\theta}}+\boldsymbol{C}(\boldsymbol{\theta},\dot{\boldsymbol{\theta}})\dot{\boldsymbol{\theta}}+\boldsymbol{G}(\boldsymbol{\theta})+\boldsymbol{d}_t(t)-\boldsymbol{J}^{\mathrm{T}}(\boldsymbol{\theta})\Delta\boldsymbol{F}_{m0}(\boldsymbol{x}_m,\boldsymbol{p})\\&\quad+\boldsymbol{J}^{\mathrm{T}}(\boldsymbol{\theta})\boldsymbol{F}_{mf0}(\boldsymbol{x}_m,\dot{\boldsymbol{x}}_m,\boldsymbol{p})+\boldsymbol{J}^{\mathrm{T}}(\boldsymbol{\theta})\Delta\boldsymbol{F}_{mf}(\boldsymbol{x}_m,\dot{\boldsymbol{x}}_m,\boldsymbol{p})\\&\quad=\boldsymbol{J}^{\mathrm{T}}(\boldsymbol{\theta})\boldsymbol{F}_{m0}(\boldsymbol{x}_m,\boldsymbol{p}).\end{aligned}\tag{5}$$

It is noted that the following properties hold in (5) [22].

a) $\boldsymbol{M}(\boldsymbol{\theta})$ is a symmetric positive definite matrix and there exist positive values k_{m1} and k_{m2} such that $k_{m1}\boldsymbol{I}_n \le \boldsymbol{M}(\boldsymbol{\theta}) \le k_{m2}\boldsymbol{I}_n$.
b) $\boldsymbol{N}(\boldsymbol{\theta},\dot{\boldsymbol{\theta}})$, which is defined as $\boldsymbol{N}(\boldsymbol{\theta},\dot{\boldsymbol{\theta}}) = \dot{\boldsymbol{M}}(\boldsymbol{\theta}) - 2\boldsymbol{C}(\boldsymbol{\theta},\dot{\boldsymbol{\theta}})$, is a skew-symmetric matrix.

For notation simplicity, define the virtual drive moment of the parallel manipulator as

$$\boldsymbol{\tau}=\boldsymbol{J}^{\mathrm{T}}(\boldsymbol{\theta})\boldsymbol{F}_{m0}(\boldsymbol{x}_m,\boldsymbol{p})=\boldsymbol{f}_t(\boldsymbol{\theta})\boldsymbol{p}+\boldsymbol{g}_t(\boldsymbol{\theta})\tag{6}$$

where $\boldsymbol{f}_t(\boldsymbol{\theta}) = \boldsymbol{J}^{\mathrm{T}}(\boldsymbol{\theta})\operatorname{diag}(A_i(x_{mi}))$, $\boldsymbol{g}_t(\boldsymbol{\theta}) = \boldsymbol{J}^{\mathrm{T}}(\boldsymbol{\theta})F_{ri}(x_{mi})$.

B. Dynamics of Actuator

The dynamics of actuator, i.e., the pressure dynamics can be described as [13]

$$\dot{\boldsymbol{p}}=\boldsymbol{g}_p(\boldsymbol{x}_m,\dot{\boldsymbol{x}}_m,\boldsymbol{p})+\boldsymbol{f}_p(\boldsymbol{x}_m)\boldsymbol{q}_m+\boldsymbol{d}_p(t)\tag{7}$$

where $\boldsymbol{g}_p(\boldsymbol{x}_m,\dot{\boldsymbol{x}}_m,\boldsymbol{p})$, and $\boldsymbol{f}_p(\boldsymbol{x}_m)$ are nonlinear matrices, $\boldsymbol{q}_m$ is the average flow rate through the fast switching valves, and $\boldsymbol{d}_p(t)$ is the overall disturbance vector in muscle-space.

The average flow rate $\boldsymbol{q}_m$ through the fast switching valves is determined as [12]

$$\boldsymbol{q}_m(\boldsymbol{u})=\boldsymbol{K}_q(\boldsymbol{p})\boldsymbol{u}\tag{8}$$

where $\boldsymbol{K}_q(\boldsymbol{p})$ is a diagonal matrix of nonlinear flow gain functions, $\boldsymbol{u}$ is the duty cycle vector of fast switching valves. It is noted that the model error between the actual flow rate and the average flow rate is also lumped into $\boldsymbol{d}_p(t)$, which will be attenuated by robust feedback later.

C. System Dynamics

Merging (5)–(8), the entire system dynamics can be written as

$$\begin{cases}\boldsymbol{M}(\boldsymbol{\theta})\ddot{\boldsymbol{\theta}}+\boldsymbol{C}(\boldsymbol{\theta},\dot{\boldsymbol{\theta}})\dot{\boldsymbol{\theta}}+\boldsymbol{G}(\boldsymbol{\theta})+\boldsymbol{d}_t(t)-\boldsymbol{J}^{\mathrm{T}}(\boldsymbol{\theta})\Delta\boldsymbol{F}_{m0}(\boldsymbol{x}_m,\boldsymbol{p})\\\quad+\boldsymbol{J}^{\mathrm{T}}(\boldsymbol{\theta})\boldsymbol{F}_{mf0}(\boldsymbol{x}_m,\dot{\boldsymbol{x}}_m,\boldsymbol{p})+\boldsymbol{J}^{\mathrm{T}}(\boldsymbol{\theta})\Delta\boldsymbol{F}_{mf}(\boldsymbol{x}_m,\dot{\boldsymbol{x}}_m,\boldsymbol{p})\\\quad=\boldsymbol{\tau}=\boldsymbol{f}_{\mathrm{t}}(\boldsymbol{\theta})\boldsymbol{p}+\boldsymbol{g}_t(\boldsymbol{\theta})\\\dot{\boldsymbol{p}}=\boldsymbol{g}_p(\boldsymbol{x}_m,\dot{\boldsymbol{x}}_m,\boldsymbol{p})+\boldsymbol{f}_p(\boldsymbol{x}_m)\boldsymbol{K}_q(\boldsymbol{p})\boldsymbol{u}+\boldsymbol{d}_p(t).\end{cases}\tag{9}$$

III. Parameter Estimation Algorithm

Let $\boldsymbol{\beta}$ be the unknown parameter vector and $\tilde{\boldsymbol{\beta}}$ the parameter estimation error. The parameter estimation is to construct suitable estimation function $\boldsymbol{\sigma}$ so that an improved final tracking accuracy can be obtained with an emphasis on good parameter estimation process as well [23]. The nonlinear disturbances of (9) can be decomposed into unknown constant nominal values and time-varying uncertainties respectively, i.e., $\boldsymbol{d}_t = \boldsymbol{d}_{t0} + \tilde{\boldsymbol{d}}_t$ and $\boldsymbol{d}_p = \boldsymbol{d}_{p0} + \tilde{\boldsymbol{d}}_p$. $\boldsymbol{d}_{p0}$ and $\boldsymbol{d}_{t0}$ will be obtained through online parameter estimation.

A. Projection Type Adaptation Law

The prior process knowledge such as the physical bounds of the parameters is used to construct projection type adaptation law for a controlled learning process even in the presence of disturbances. As in [14], [23], the widely used projection mapping $\operatorname{Proj}_{\hat{\boldsymbol{\beta}}}(\boldsymbol{\zeta})$ will be used to keep the parameter estimates within the known bounded convex set $\bar{\Omega}_{\boldsymbol{\beta}}$, the closure of the convex set $\Omega_{\boldsymbol{\beta}} = \{\boldsymbol{\beta} : \boldsymbol{\beta}_{\min} \le \boldsymbol{\beta} \le \boldsymbol{\beta}_{\max}\}$. The standard projection mapping is

$$\operatorname{Proj}_{\hat{\boldsymbol{\beta}}}(\boldsymbol{\zeta})=\begin{cases}\boldsymbol{\zeta}, & \text{if } \hat{\boldsymbol{\beta}}\in\mathring{\Omega}_{\boldsymbol{\beta}} \text{ or } \boldsymbol{n}_{\hat{\boldsymbol{\beta}}}^{\mathrm{T}}\boldsymbol{\zeta}\le 0\\\left(1-\boldsymbol{\gamma}\dfrac{\boldsymbol{n}_{\hat{\boldsymbol{\beta}}}\boldsymbol{n}_{\hat{\boldsymbol{\beta}}}^{\mathrm{T}}}{\boldsymbol{n}_{\hat{\boldsymbol{\beta}}}^{\mathrm{T}}\boldsymbol{\gamma}\boldsymbol{n}_{\hat{\boldsymbol{\beta}}}}\right)\boldsymbol{\zeta}, & \text{if } \hat{\boldsymbol{\beta}}\in\partial\Omega_{\boldsymbol{\beta}} \text{ or } \boldsymbol{n}_{\hat{\boldsymbol{\beta}}}^{\mathrm{T}}\boldsymbol{\zeta}>0\end{cases}\tag{10}$$

where $\boldsymbol{\zeta} \in R^p$ is any function and $\boldsymbol{\gamma}(t) \in R^{p\times p}$ can be any time-varying positive definite symmetric matrix. $\mathring{\Omega}_{\boldsymbol{\beta}}$ and $\partial\Omega_{\boldsymbol{\beta}}$ denote the interior and the boundary of $\Omega_{\boldsymbol{\beta}}$, respectively, and $\boldsymbol{n}_{\hat{\boldsymbol{\beta}}}$ represents the outward unit normal vector at $\hat{\boldsymbol{\beta}} \in \partial\Omega_{\boldsymbol{\beta}}$.

To achieve a complete separation of estimator design and robust control law design, in addition to the projection type adaptation law (10), it is also necessary to use the preset adaptation rate limits for a controlled estimation process. Therefore, a saturation function is defined as [14]

$$\operatorname{sat}_{\dot{\boldsymbol{\beta}}_M}(\boldsymbol{\zeta})=s_0\boldsymbol{\zeta},\quad \boldsymbol{s}_0=\begin{cases}1, & \|\boldsymbol{\zeta}\|\le\dot{\boldsymbol{\beta}}_M\\\dfrac{\dot{\boldsymbol{\beta}}_M}{\|\boldsymbol{\zeta}\|}, & \|\boldsymbol{\zeta}\|>\dot{\boldsymbol{\beta}}_M\end{cases}\tag{11}$$

where $\dot{\boldsymbol{\beta}}_M$ is the preset adaptation rate limit.

The parameter estimate $\hat{\boldsymbol{\beta}}$ is updated using the following projection type adaptation law with the preset adaptation rate limit $\dot{\boldsymbol{\beta}}_M$:

$$\dot{\hat{\boldsymbol{\beta}}} = \mathrm{sat}_{\dot{\boldsymbol{\beta}}_M}\left(\mathrm{Proj}_{\hat{\boldsymbol{\beta}}}(\boldsymbol{\gamma}\boldsymbol{\sigma})\right), \quad \hat{\boldsymbol{\beta}}(0) \in \Omega_{\boldsymbol{\beta}} \tag{12}$$

where $\boldsymbol{\sigma}$ is any adaptation function and $\boldsymbol{\gamma}$ is the adaptation rate matrix, which can be any continuously differentiable positive symmetric matrix. With the above adaptation law structure, the following properties will be hold [14], [23], [24].

P1: The parameter estimates are always within the known bounded set, i.e., $\hat{\boldsymbol{\beta}}(t) \in \Omega_{\boldsymbol{\beta}} = \left\{\hat{\boldsymbol{\beta}} : \boldsymbol{\beta}_{\min} \le \hat{\boldsymbol{\beta}} \le \boldsymbol{\beta}_{\max}\right\}$, $\forall\, t$.

P2:

$$\tilde{\boldsymbol{\beta}}^{\mathrm{T}}\left[\boldsymbol{\gamma}^{-1}\mathrm{Proj}_{\hat{\boldsymbol{\beta}}}(\boldsymbol{\gamma}\boldsymbol{\sigma}) - \boldsymbol{\sigma}\right] \le 0, \quad \forall\, \boldsymbol{\sigma}. \tag{13}$$

P3: The parameter update rate is uniformly bounded by $\left|\dot{\hat{\boldsymbol{\beta}}}(t)\right| \le \dot{\boldsymbol{\beta}}_M, \forall\, t$.

As seen from the previous properties, the parameter estimates and their derivatives are bounded with known bounds, regardless of the estimation function $\boldsymbol{\sigma}$ to be used. Such a fact will be used in the following for a complete separation of the robust control law design from the parameter adaptation process.

B. Prediction Errors of Parameter Estimation for Parallel Manipulator

Let $\boldsymbol{\beta}_r$ be the parameter vector used for $\boldsymbol{M}(\boldsymbol{\theta})$, $\boldsymbol{C}(\boldsymbol{\theta},\dot{\boldsymbol{\theta}})$, $\boldsymbol{G}(\boldsymbol{\theta})$, and $\boldsymbol{d}_{t0}$ in (5) and denote $\boldsymbol{\beta}_{\mathrm{ma}} = [a_0, a_1, a_2, a_3, b_0, b_1, b_2, b_3, a_{f0}, a_{f1}, a_{f2}, a_{f3}, b_{f0}, b_{f1}, b_{f2}, b_{f3}]^{\mathrm{T}}$. If the system model in (9) is directly used to obtain the parameter estimation algorithm, acceleration feedback and the pressure changing rate would be needed. Though these signals could be obtained through numerical differentiation of velocity and pressure feedback signals, severe noise influences will be inevitable. To bypass this problem, stable filters will be employed to obtain suitable regression model for parameter estimation as follows.

Equation (5) is rewritten as the following form:

$$\begin{aligned}&\frac{d}{dt}\left[\boldsymbol{M}(\boldsymbol{\theta})\dot{\boldsymbol{\theta}}\right] - \boldsymbol{C}^{\mathrm{T}}(\boldsymbol{\theta},\dot{\boldsymbol{\theta}})\dot{\boldsymbol{\theta}} + \boldsymbol{G}(\boldsymbol{\theta}) + \boldsymbol{d}_t\\ &\quad + \boldsymbol{\varphi}_{ma}^{\mathrm{T}}(\boldsymbol{\theta},\boldsymbol{x}_m,\dot{\boldsymbol{x}}_m,\boldsymbol{p})\boldsymbol{\beta}_{ma}\\ &\quad + \boldsymbol{J}^{\mathrm{T}}(\boldsymbol{\theta})\boldsymbol{F}_{mf0}(\boldsymbol{x}_m,\dot{\boldsymbol{x}}_m,\boldsymbol{p}) = \boldsymbol{\tau}\end{aligned} \tag{14}$$

where $\boldsymbol{\varphi}_{ma}(\boldsymbol{\theta},\boldsymbol{x}_m,\dot{\boldsymbol{x}}_m,\boldsymbol{p}) = [\boldsymbol{J}^{\mathrm{T}}(\boldsymbol{\theta})\boldsymbol{\varphi}_{mF}(\boldsymbol{x}_m,\boldsymbol{p}), -\boldsymbol{J}^{\mathrm{T}}(\boldsymbol{\theta})\boldsymbol{S}_x(\dot{\boldsymbol{x}}_m)\boldsymbol{\varphi}_{mF}(\boldsymbol{x}_m,\boldsymbol{p})]^{\mathrm{T}}$, $\boldsymbol{\varphi}_{mF}$

$$(\boldsymbol{x}_m,\boldsymbol{p}) = -\begin{bmatrix} p_1, x_{m1}p_1, x_{m1}^2p_1, x_{m1}^3p_1, 1, x_{m1}, x_{m1}^2, x_{m1}^3 \\ p_2, x_{m2}p_2, x_{m2}^2p_2, x_{m2}^3p_2, 1, x_{m2}, x_{m2}^2, x_{m2}^3 \\ p_3, x_{m3}p_3, x_{m3}^2p_3, x_{m3}^3p_3, 1, x_{m3}, x_{m3}^2, x_{m3}^3 \end{bmatrix}$$

$\boldsymbol{S}_x(\dot{\boldsymbol{x}}_m) = \mathrm{diag}([\mathrm{sign}(\dot{x}_{m1}), \mathrm{sign}(\dot{x}_{m2}), \mathrm{sign}(\dot{x}_{m3})]^{\mathrm{T}})$.

Let $H_f(s)$ be the stable filter with a relative degree larger than or equal to 1 [23]. For example, let

$$H_f(s) = \frac{\chi}{s+\chi} \tag{15}$$

where χ is the parameter of the filter. Then, when $\tilde{\boldsymbol{d}}_t = 0$, applying the filter to both sides of (14), one obtains

$$\begin{aligned}&\left\{\frac{d}{dt}\left[\boldsymbol{M}(\boldsymbol{\theta})\dot{\boldsymbol{\theta}}\right]\right\}_f + \left\{-\boldsymbol{C}^{\mathrm{T}}(\boldsymbol{\theta},\dot{\boldsymbol{\theta}})\dot{\boldsymbol{\theta}} + \boldsymbol{G}(\boldsymbol{\theta}) + \boldsymbol{d}_{t0}\right\}_f\\ &\quad + \boldsymbol{\varphi}_{\mathrm{maf}}^{\mathrm{T}}(\boldsymbol{\theta},\boldsymbol{x}_m,\dot{\boldsymbol{x}}_m,\boldsymbol{p})\boldsymbol{\beta}_{ma}\\ &\quad + \left\{\boldsymbol{J}^{\mathrm{T}}(\boldsymbol{\theta})\boldsymbol{F}_{mf0}(\boldsymbol{x}_m,\dot{\boldsymbol{x}}_m,\boldsymbol{p})\right\}_f = \boldsymbol{\tau}_f\end{aligned} \tag{16}$$

where $\left\{d/dt\left[\boldsymbol{M}(\boldsymbol{\theta})\dot{\boldsymbol{\theta}}\right]\right\}_f$, $\left\{-\boldsymbol{C}^{\mathrm{T}}(\boldsymbol{\theta},\dot{\boldsymbol{\theta}})\dot{\boldsymbol{\theta}} + \boldsymbol{G}(\boldsymbol{\theta}) + \boldsymbol{d}_{t0}\right\}_f$, $\boldsymbol{\varphi}_{\mathrm{maf}}(\boldsymbol{\theta},\boldsymbol{x}_m,\dot{\boldsymbol{x}}_m,\boldsymbol{p})$, $\left\{\boldsymbol{J}^{\mathrm{T}}(\boldsymbol{\theta})\boldsymbol{F}_{mf0}(\boldsymbol{x}_m,\dot{\boldsymbol{x}}_m,\boldsymbol{p})\right\}_f$, and $\boldsymbol{\tau}_f$ represent the filtered $d/dt\left[\boldsymbol{M}(\boldsymbol{\theta})\dot{\boldsymbol{\theta}}\right]$, $-\boldsymbol{C}^{\mathrm{T}}(\boldsymbol{\theta},\dot{\boldsymbol{\theta}})\dot{\boldsymbol{\theta}} + \boldsymbol{G}(\boldsymbol{\theta}) + \boldsymbol{d}_{t0}$, $\boldsymbol{\varphi}_{ma}(\boldsymbol{\theta},\boldsymbol{x}_m,\dot{\boldsymbol{x}}_m,\boldsymbol{p})$, $\boldsymbol{J}^{\mathrm{T}}(\boldsymbol{\theta})\boldsymbol{F}_{mf0}(\boldsymbol{x}_m,\dot{\boldsymbol{x}}_m,\boldsymbol{p})$, and $\boldsymbol{\tau}$, respectively.

Let $\left\{d/dt\left[\boldsymbol{M}(\boldsymbol{\theta})\dot{\boldsymbol{\theta}}\right]\right\}_f + \left\{-\boldsymbol{C}^{\mathrm{T}}(\boldsymbol{\theta},\dot{\boldsymbol{\theta}})\dot{\boldsymbol{\theta}} + \boldsymbol{G}(\boldsymbol{\theta}) + \boldsymbol{d}_{t0}\right\}_f = \boldsymbol{\varphi}_{rf}^{\mathrm{T}}(\boldsymbol{\theta},\dot{\boldsymbol{\theta}})\boldsymbol{\beta}_r + \boldsymbol{y}_{rf}(\boldsymbol{\theta},\dot{\boldsymbol{\theta}})$, $\boldsymbol{\varphi}_{\mathrm{maf}}^{\mathrm{T}}(\boldsymbol{\theta},\boldsymbol{x}_m,\dot{\boldsymbol{x}}_m,\boldsymbol{p})\boldsymbol{\beta}_{ma} + \left\{\boldsymbol{J}^{\mathrm{T}}(\boldsymbol{\theta})\boldsymbol{F}_{mf0}(\boldsymbol{x}_m,\dot{\boldsymbol{x}}_m,\boldsymbol{p})\right\}_f = \boldsymbol{\varphi}_{mf}^{\mathrm{T}}(\boldsymbol{\theta},\boldsymbol{x}_m,\dot{\boldsymbol{x}}_m,\boldsymbol{p})\boldsymbol{\beta}_m + \boldsymbol{y}_{mf}(\boldsymbol{\theta},\boldsymbol{x}_m,\dot{\boldsymbol{x}}_m,\boldsymbol{p})$, and substitute them into (16) while noting that $\dot{\boldsymbol{x}}_m$ is a function of $\boldsymbol{\theta}$ and $\dot{\boldsymbol{\theta}}$. Then, a linear regression model can be given by

$$\begin{aligned}&\boldsymbol{\varphi}_{rf}^{\mathrm{T}}(\boldsymbol{\theta},\dot{\boldsymbol{\theta}})\boldsymbol{\beta}_r + \boldsymbol{y}_{rf}(\boldsymbol{\theta},\dot{\boldsymbol{\theta}})\\ &\qquad + \boldsymbol{\varphi}_{mf}^{\mathrm{T}}(\boldsymbol{\theta},\dot{\boldsymbol{\theta}},\boldsymbol{p})\boldsymbol{\beta}_m + \boldsymbol{y}_{mf}(\boldsymbol{\theta},\dot{\boldsymbol{\theta}},\boldsymbol{p}) = \boldsymbol{\tau}_f\end{aligned} \tag{17}$$

where $\boldsymbol{\varphi}_{rf}(\boldsymbol{\theta},\dot{\boldsymbol{\theta}})$ is the corresponding regressor of $\boldsymbol{\beta}_r$, $\boldsymbol{y}_{rf}(\boldsymbol{\theta},\dot{\boldsymbol{\theta}})$ is a known nonlinear term, $\boldsymbol{\beta}_m$ represents the unknown parameters of $\boldsymbol{\beta}_{ma}$, $\boldsymbol{\varphi}_{\mathrm{mf}}(\boldsymbol{\theta},\dot{\boldsymbol{\theta}},\boldsymbol{p})$ is the corresponding regressor of $\boldsymbol{\beta}_m$, and $\boldsymbol{y}_{mf}(\boldsymbol{\theta},\dot{\boldsymbol{\theta}},\boldsymbol{p})$ is a known nonlinear term.

From (17), the basic regression model for physical dynamics of the parallel manipulator can be given by

$$\boldsymbol{y}_1 = \boldsymbol{\varphi}_1^{\mathrm{T}}(\boldsymbol{\theta},\dot{\boldsymbol{\theta}},\boldsymbol{p})\boldsymbol{\beta}_t \tag{18}$$

where $\boldsymbol{\beta}_t = [\boldsymbol{\beta}_r^{\mathrm{T}}, \boldsymbol{\beta}_m^{\mathrm{T}}]^{\mathrm{T}}$, $\boldsymbol{\varphi}_1(\boldsymbol{\theta},\dot{\boldsymbol{\theta}},\boldsymbol{p}) = [\boldsymbol{\varphi}_{rf}^{\mathrm{T}}(\boldsymbol{\theta},\dot{\boldsymbol{\theta}}), \boldsymbol{\varphi}_{mf}^{\mathrm{T}}(\boldsymbol{\theta},\dot{\boldsymbol{\theta}},\boldsymbol{p})]^{\mathrm{T}}$, $\boldsymbol{y}_1 = \boldsymbol{\tau}_f - \boldsymbol{y}_{rf}(\boldsymbol{\theta},\dot{\boldsymbol{\theta}}) - \boldsymbol{y}_{mf}(\boldsymbol{\theta},\dot{\boldsymbol{\theta}},\boldsymbol{p})$.

Let $\boldsymbol{\eta}_1 = \hat{\boldsymbol{y}}_1 - \boldsymbol{y}_1$, where $\hat{\boldsymbol{y}}_1 = \boldsymbol{\varphi}_1^{\mathrm{T}}(\boldsymbol{\theta},\dot{\boldsymbol{\theta}},\boldsymbol{p})\hat{\boldsymbol{\beta}}_t$. Then the prediction error $\boldsymbol{\eta}_1$ related to the parameter estimation error is expressed as

$$\boldsymbol{\eta}_1 = \varphi_1^{\mathrm{T}}(\boldsymbol{\theta},\dot{\boldsymbol{\theta}},p)\tilde{\beta}_t = \varphi_1^{\mathrm{T}}(\boldsymbol{\theta},\dot{\boldsymbol{\theta}},p)\hat{\boldsymbol{\beta}}_t - \boldsymbol{y}_1. \tag{19}$$

Theoretically, the linear regression model (19) is the standard form to which various traditional parameter estimation algorithms such as the least squares method can be applied for the parameter estimates $\hat{\boldsymbol{\beta}}_t$. However, since there are a large number of parameters $\boldsymbol{\beta}_t$ to be identified and there are not-so-rich desired posture trajectories to be tracked, the persistent exciting conditions, which are required for the convergence of online parameter estimation, are hard to be satisfied all the time. As a result, unreliable and inaccurate parameter estimations with large covariance may sometimes appear due to the unavoidable model errors in reality, and will lead to poor control performance in implementation. To solve this practical problem, additional practical constraints are imposed to further condition the parameter estimation process for obtaining reliable estimates of effective model parameters. As a feasible method, parameter estimates $\hat{\boldsymbol{\beta}}_t$ are required to minimize not only the prediction error $\boldsymbol{\eta}_1$ but also

the correction term of static force ΔF_{m0} and the pressure gain ΔA in (3). Specifically, from (3), ΔF_{m0} and ΔA are linear in terms of $\boldsymbol{\beta}_t$ and can be rewritten as follows in the form of linear regression:

$$\Delta \boldsymbol{F}_{m0} = \boldsymbol{\varphi}_2^{\mathrm{T}}(\boldsymbol{\theta}, \boldsymbol{p})\boldsymbol{\beta}_t - \boldsymbol{y}_2 \tag{20}$$

$$\Delta \boldsymbol{A} = \boldsymbol{\varphi}_3^{\mathrm{T}}(\boldsymbol{\theta}, \boldsymbol{p})\boldsymbol{\beta}_t - \boldsymbol{y}_3 \tag{21}$$

where $\boldsymbol{\varphi}_2(\boldsymbol{\theta}, \boldsymbol{p})$ and $\boldsymbol{\varphi}_3(\boldsymbol{\theta}, \boldsymbol{p})$ are the corresponding regressor matrices of $\boldsymbol{\beta}_t$, and $\boldsymbol{y}_2$ and $\boldsymbol{y}_3$ represent all the other known terms in $\Delta \boldsymbol{F}_{m0}$ and $\Delta \boldsymbol{A}$, respectively. Thus, minimizing $\Delta \hat{\boldsymbol{F}}_{m0}$ and $\Delta \hat{\boldsymbol{A}}$ are equivalent to minimizing the following prediction errors respectively:

$$\boldsymbol{\eta}_2 = \boldsymbol{\varphi}_2^{\mathrm{T}}(\boldsymbol{\theta}, \boldsymbol{p})\hat{\boldsymbol{\beta}}_t - \boldsymbol{y}_2 \tag{22}$$

$$\boldsymbol{\eta}_3 = \boldsymbol{\varphi}_3^{\mathrm{T}}(\boldsymbol{\theta}, \boldsymbol{p})\hat{\boldsymbol{\beta}}_t - \boldsymbol{y}_3. \tag{23}$$

Overall, the parameter estimates $\hat{\beta}_t$ will be determined by minimizing a composite error that is a weighted function of the above three prediction errors $\boldsymbol{\eta}_1$, $\boldsymbol{\eta}_2$, and $\boldsymbol{\eta}_3$.

C. Parameter Estimation Algorithm Based on Composite Error Minimizing Criterion for Parallel Manipulator

The composite error minimizing criterion given by (24) takes into account all the three prediction errors in (19), (22) and (23) [25]

$$\begin{aligned} V(\hat{\boldsymbol{\beta}}_t) = {} & \omega_1 \int_0^t e^{-\alpha_1(t-\tau)} \left(\boldsymbol{\varphi}_1^{\mathrm{T}}(\tau)\hat{\boldsymbol{\beta}}_t - \boldsymbol{y}_1(\tau)\right)^{\mathrm{T}} \\ & \times \left(\boldsymbol{\varphi}_1^{\mathrm{T}}(\tau)\hat{\boldsymbol{\beta}}_t - \boldsymbol{y}_1(\tau)\right) d\tau \\ & + \omega_2 \int_0^t e^{-\alpha_2(t-\tau)} \left(\boldsymbol{\varphi}_2^{\mathrm{T}}(\tau)\hat{\boldsymbol{\beta}}_t - \boldsymbol{y}_2(\tau)\right)^{\mathrm{T}} \\ & \times \left(\boldsymbol{\varphi}_2^{\mathrm{T}}(\tau)\hat{\boldsymbol{\beta}}_t - \boldsymbol{y}_2(\tau)\right) d\tau \\ & + \omega_3 \int_0^t e^{-\alpha_3(t-\tau)} \left(\boldsymbol{\varphi}_3^{\mathrm{T}}(\tau)\hat{\boldsymbol{\beta}}_t - \boldsymbol{y}_3(\tau)\right)^{\mathrm{T}} \\ & \times \left(\boldsymbol{\varphi}_3^{\mathrm{T}}(\tau)\hat{\boldsymbol{\beta}}_t - \boldsymbol{y}_3(\tau)\right) d\tau \end{aligned} \tag{24}$$

where $\alpha_i \geq 0$, $(i = 1, 2, 3)$ are the forgetting factors and $\omega_i \geq 0$, $(i = 1, 2, 3)$ are the weights.

The optimal parameter vector is then determined such that the above performance index is minimized, which leads to the following necessary condition:

$$\left.\frac{\partial V}{\partial \hat{\boldsymbol{\beta}}_t}\right|_{\hat{\boldsymbol{\beta}}_t} = 0. \tag{25}$$

Equation (25) is equivalent to

$$\begin{aligned} & \omega_1 \left(\int_0^t e^{-\alpha_1(t-\tau)}\boldsymbol{\varphi}_1(\tau)\boldsymbol{\varphi}_1^{\mathrm{T}}(\tau)d\tau\right)\hat{\boldsymbol{\beta}}_t(t) \\ & + \omega_2 \left(\int_0^t e^{-\alpha_2(t-\tau)}\boldsymbol{\varphi}_2(\tau)\boldsymbol{\varphi}_2^{\mathrm{T}}(\tau)d\tau\right)\hat{\boldsymbol{\beta}}_t(t) \\ & + \omega_3 \left(\int_0^t e^{-\alpha_3(t-\tau)}\boldsymbol{\varphi}_3(\tau)\boldsymbol{\varphi}_3^{\mathrm{T}}(\tau)d\tau\right)\hat{\boldsymbol{\beta}}_t(t) \\ & = \omega_1 \int_0^t e^{-\alpha_1(t-\tau)}\boldsymbol{\varphi}_1(\tau)\boldsymbol{y}_1(\tau)d\tau \\ & + \omega_2 \int_0^t e^{-\alpha_2(t-\tau)}\boldsymbol{\varphi}_2(\tau)\boldsymbol{y}_2(\tau)d\tau \\ & + \omega_3 \int_0^t e^{-\alpha_3(t-\tau)}\boldsymbol{\varphi}_3(\tau)\boldsymbol{y}_3(\tau)d\tau. \end{aligned} \tag{26}$$

The time derivative of (26) is

$$\begin{aligned} & \omega_1\boldsymbol{\varphi}_1(t)\boldsymbol{\varphi}_1^{\mathrm{T}}(t)\hat{\boldsymbol{\beta}}_{\mathrm{t}}(t) \\ & + \omega_1 \left(\int_0^t e^{-\alpha_1(t-\tau)}\boldsymbol{\varphi}_1(\tau)\boldsymbol{\varphi}_1^{\mathrm{T}}(\tau)d\tau\right)\frac{d\hat{\boldsymbol{\beta}}_t(t)}{dt} \\ & + \omega_2\boldsymbol{\varphi}_2(t)\boldsymbol{\varphi}_2^{\mathrm{T}}(t)\hat{\boldsymbol{\beta}}_t(t) \\ & + \omega_2 \left(\int_0^t e^{-\alpha_2(t-\tau)}\boldsymbol{\varphi}_2(\tau)\boldsymbol{\varphi}_2^{\mathrm{T}}(\tau)d\tau\right)\frac{d\hat{\boldsymbol{\beta}}_t(t)}{dt} \\ & + \omega_3\boldsymbol{\varphi}_3(t)\boldsymbol{\varphi}_3^{\mathrm{T}}(t)\hat{\boldsymbol{\beta}}_t(t) \\ & + \omega_3 \left(\int_0^t e^{-\alpha_3(t-\tau)}\boldsymbol{\varphi}_3(\tau)\boldsymbol{\varphi}_3^{\mathrm{T}}(\tau)d\tau\right)\frac{d\hat{\boldsymbol{\beta}}_t(t)}{dt} \\ & = \omega_1\boldsymbol{\varphi}_1(t)\boldsymbol{y}_1(t) + \omega_2\boldsymbol{\varphi}_2(t)\boldsymbol{y}_2(t) + \omega_3\boldsymbol{\varphi}_3(t)\boldsymbol{y}_3(t). \end{aligned} \tag{27}$$

For notation simplicity, define the following equation:

$$\begin{aligned} \boldsymbol{R}_1(t) &= \int_0^t e^{-\alpha_1(t-\tau)}\boldsymbol{\varphi}_1(\tau)\boldsymbol{\varphi}_1^{\mathrm{T}}(\tau)d\tau \\ \boldsymbol{R}_2(t) &= \int_0^t e^{-\alpha_2(t-\tau)}\boldsymbol{\varphi}_2(\tau)\boldsymbol{\varphi}_2^{\mathrm{T}}(\tau)d\tau \\ \boldsymbol{R}_3(t) &= \int_0^t e^{-\alpha_3(t-\tau)}\boldsymbol{\varphi}_3(\tau)\boldsymbol{\varphi}_3^{\mathrm{T}}(\tau)d\tau \\ \boldsymbol{R}(t) &= \boldsymbol{\gamma}_1^{-1}(t) = \omega_1\boldsymbol{R}_1(t) + \omega_2\boldsymbol{R}_2(t) + \omega_3\boldsymbol{R}_3(t). \end{aligned} \tag{28}$$

From (27) and (28), the parameter adaptation law is given by (29) while noting (12)

$$\dot{\hat{\boldsymbol{\beta}}}_t = \mathrm{sat}_{\dot{\boldsymbol{\beta}}_M}\left(\mathrm{Proj}_{\hat{\boldsymbol{\beta}}}(\boldsymbol{\gamma}_1\boldsymbol{\sigma}_1)\right) \tag{29}$$

with the parameter adaptation function $\boldsymbol{\sigma}_1$ and the adaptation rate matrix $\boldsymbol{\gamma}_1$, respectively, given by

$$\boldsymbol{\sigma}_1(t) = \boldsymbol{\gamma}_1(t) + \boldsymbol{\gamma}_2(t) + \boldsymbol{\gamma}_3(t) \tag{30}$$

$$\dot{\boldsymbol{\gamma}}_1(t) = -\boldsymbol{\gamma}_1(t)\dot{\boldsymbol{R}}(t)\boldsymbol{\gamma}_1(t) \tag{31}$$

where $\boldsymbol{\gamma}_1(t) = -\omega_1\boldsymbol{\varphi}_1(t)\boldsymbol{\eta}_1(t)$, $\boldsymbol{\gamma}_2(t) = -\omega_2\boldsymbol{\varphi}_2(t)\boldsymbol{\eta}_2(t)$, $\boldsymbol{\gamma}_3(t) = -\omega_3\boldsymbol{\varphi}_3(t)\boldsymbol{\eta}_3(t)$, $\boldsymbol{\eta}_1(t) = \boldsymbol{\varphi}_1^{\mathrm{T}}(t)\hat{\boldsymbol{\beta}}_t(t) - \boldsymbol{y}_1(t)$, $\boldsymbol{\eta}_2(t) = \boldsymbol{\varphi}_2^{\mathrm{T}}(t)\hat{\boldsymbol{\beta}}_t(t) - \boldsymbol{y}_2(t)$, $\boldsymbol{\eta}_3(t) = \boldsymbol{\varphi}_3^{\mathrm{T}}(t)\hat{\boldsymbol{\beta}}_t(t) - \boldsymbol{y}_3(t)$, $\dot{\boldsymbol{R}}(t) = \omega_1\dot{\boldsymbol{R}}_1(t) + \omega_2\dot{\boldsymbol{R}}_2(t) + \omega_3\dot{\boldsymbol{R}}_3(t)$, $\dot{\boldsymbol{R}}_1(t) = -\alpha_1\boldsymbol{R}_1(t) + \boldsymbol{\varphi}_1(t)\boldsymbol{\varphi}_1^{\mathrm{T}}(t)$, $\dot{\boldsymbol{R}}_2(t) = -\alpha_2\boldsymbol{R}_2(t) + \boldsymbol{\varphi}_2(t)\boldsymbol{\varphi}_2^{\mathrm{T}}(t)$, $\dot{\boldsymbol{R}}_3(t) = -\alpha_3\boldsymbol{R}_3(t) + \boldsymbol{\varphi}_3(t)\boldsymbol{\varphi}_3^{\mathrm{T}}(t)$.

D. Parameter Estimation for Actuator

The conventional parameter estimation algorithm based on single error minimizing criterion is utilized to identify parameters of the actuator dynamics as follows.

A filter function with the same structure as $H_f(s)$ is applied to the second equation of (9) for obtaining the following regression model:

$$\dot{\boldsymbol{p}}_f = \boldsymbol{\varphi}_{pf}^{\mathrm{T}}(\boldsymbol{x}_m, \dot{\boldsymbol{x}}_m, \boldsymbol{p}, \boldsymbol{u})\boldsymbol{\beta}_p + \boldsymbol{y}_{pf}(\boldsymbol{x}_m, \dot{\boldsymbol{x}}_m, \boldsymbol{p}) \tag{32}$$

where $\dot{\boldsymbol{p}}_f$ is the filtered $\dot{\boldsymbol{p}}$, $\boldsymbol{\beta}_p$ represents the unknown parameter vector in $\boldsymbol{g}_p(\boldsymbol{x}_m, \dot{\boldsymbol{x}}_m, \boldsymbol{p})$, $\boldsymbol{f}_p(\boldsymbol{x}_m)$ and $\boldsymbol{d}_{p0}$, $\boldsymbol{\varphi}_{pf}(\boldsymbol{x}_m, \dot{\boldsymbol{x}}_m, \boldsymbol{p}, \boldsymbol{u})$ is the filtered corresponding regressor matrix, and $\boldsymbol{y}_{pf}(\boldsymbol{x}_m, \dot{\boldsymbol{x}}_m, \boldsymbol{p})$ is the filtered output of all the other known terms.

Equation (32) can also be written as follows in the form of standard linear regression model:

$$\boldsymbol{y}_4 = \boldsymbol{\varphi}_4^{\mathrm{T}}(\boldsymbol{x}_m, \dot{\boldsymbol{x}}_m, \boldsymbol{p}, \boldsymbol{u})\boldsymbol{\beta}_p \tag{33}$$

where $\boldsymbol{y}_4 = \dot{\boldsymbol{p}}_f - \boldsymbol{y}_{pf}$ and $\varphi_4(\boldsymbol{x}_m, \dot{\boldsymbol{x}}_m, \boldsymbol{p}, \boldsymbol{u}) = \boldsymbol{\varphi}_{pf}(\boldsymbol{x}_m, \dot{\boldsymbol{x}}_m, \boldsymbol{p}, \boldsymbol{u})$.

Let $\hat{\boldsymbol{y}}_4 = \boldsymbol{\varphi}_4^{\mathrm{T}}(\boldsymbol{x}_m, \dot{\boldsymbol{x}}_m, \boldsymbol{p}, \boldsymbol{u})\hat{\boldsymbol{\beta}}_p$ and $\boldsymbol{\eta}_4 = \hat{\boldsymbol{y}}_4 - \boldsymbol{y}_4$ be the predicted output and the prediction error, respectively. Then

$$\boldsymbol{\eta}_4 = \boldsymbol{\varphi}_4^{\mathrm{T}}(\boldsymbol{x}_m, \dot{\boldsymbol{x}}_m, \boldsymbol{p}, \boldsymbol{u})\tilde{\boldsymbol{\beta}}_p = \boldsymbol{\varphi}_4^{\mathrm{T}}(\boldsymbol{x}_m, \dot{\boldsymbol{x}}_m, \boldsymbol{p}, \boldsymbol{u})\hat{\boldsymbol{\beta}}_p - \boldsymbol{y}_4 \tag{34}$$

which is in the standard form that various traditional parameter estimation algorithms can be applied to for obtaining the parameter estimates $\hat{\boldsymbol{\beta}}_p$. For example, when the least squares type estimation algorithm [23] is used, $\dot{\hat{\boldsymbol{\beta}}}_p$ is updated by an adaptation law similar to the form of (12), i.e.,

$$\dot{\hat{\boldsymbol{\beta}}}_p = \mathrm{sat}_{\dot{\boldsymbol{\beta}}_M}\left(\mathrm{Proj}_{\hat{\boldsymbol{\beta}}}(\boldsymbol{\gamma}_4\boldsymbol{\sigma}_4)\right) \tag{35}$$

with the adaptation function given by

$$\boldsymbol{\sigma}_4 = -\frac{1}{1 + v\mathrm{tr}\{\boldsymbol{\varphi}_4^{\mathrm{T}}\boldsymbol{\gamma}_4\boldsymbol{\varphi}_4\}}\boldsymbol{\varphi}_4\boldsymbol{\eta}_4 \tag{36}$$

and the adaptation rate matrix given by

$$\dot{\boldsymbol{\gamma}}_4 = \alpha_4\boldsymbol{\gamma}_4 - \frac{1}{1 + v\mathrm{tr}\{\boldsymbol{\varphi}_4^{\mathrm{T}}\boldsymbol{\varphi}_4\}}\boldsymbol{\gamma}_4\boldsymbol{\varphi}_4\boldsymbol{\varphi}_4^{\mathrm{T}}\boldsymbol{\gamma}_4 \tag{37}$$

where $\alpha_4 \geq 0$ is the forgetting factor, $v \geq 0$ with $v = 0$ leading to the unnormalized algorithm.

IV. Integrated DIARC Design

In this section, an integrated DIARC that uses the online parameter estimation in Section III will be synthesized for the system (9) to achieve a guaranteed transient and final tracking accuracy. Since there exist unmatched model uncertainties in (9), backstepping design is used as in [14] and [26].

A. Integrated DIARC Design

Step 1: Define a switching-function-like quantity as

$$\boldsymbol{z}_2 = \dot{\boldsymbol{z}}_1 + \boldsymbol{K}_c\boldsymbol{z}_1 \tag{38}$$

where $\boldsymbol{z}_1 = \boldsymbol{\theta} - \boldsymbol{\theta}_d$ is the trajectory tracking error vector and $\boldsymbol{K}_c$ is a positive diagonal feedback matrix. If $\boldsymbol{z}_2$ converges to a small value or zero, then $\boldsymbol{z}_1$ will converge to a small value or zero since the transfer function from $\boldsymbol{z}_2$ to $\boldsymbol{z}_1$ is stable. Thus, the next objective is to design virtual drive moment $\boldsymbol{\tau}$ for making $\boldsymbol{z}_2$ as small as possible. For this purpose, define $\dot{\boldsymbol{\theta}}_r \triangleq \dot{\boldsymbol{\theta}}_d - \boldsymbol{K}_c\boldsymbol{z}_1$ and then the left two parts of the parallel manipulator dynamics in (9) are expressed as the form of parametric uncertainties

$$\begin{aligned}&\boldsymbol{M}(\boldsymbol{\theta})\ddot{\boldsymbol{\theta}}_r + \boldsymbol{C}(\boldsymbol{\theta}, \dot{\boldsymbol{\theta}})\dot{\boldsymbol{\theta}}_r + \boldsymbol{G}(\boldsymbol{\theta}) + \boldsymbol{d}_{t0}\\ &\quad = \boldsymbol{\varphi}_{c1}^{\mathrm{T}}(\boldsymbol{\theta}, \dot{\boldsymbol{\theta}}, \dot{\boldsymbol{\theta}}_r, \ddot{\boldsymbol{\theta}}_r)\beta_r + \boldsymbol{Y}_{c1}(\boldsymbol{\theta}, \dot{\boldsymbol{\theta}}, \dot{\boldsymbol{\theta}}_r, \ddot{\boldsymbol{\theta}}_r)\end{aligned} \tag{39}$$

$$\begin{aligned}&-\boldsymbol{J}^{\mathrm{T}}(\boldsymbol{\theta})\Delta\boldsymbol{F}_{m0}(\boldsymbol{x}_m, \boldsymbol{p}) + \boldsymbol{J}^{\mathrm{T}}(\boldsymbol{\theta})\boldsymbol{F}_{mf0}(\boldsymbol{x}_m, \dot{\boldsymbol{x}}_m, \boldsymbol{p})\\ &\quad + \boldsymbol{J}^{\mathrm{T}}(\boldsymbol{\theta})\Delta\boldsymbol{F}_{mf}(\boldsymbol{x}_m, \dot{\boldsymbol{x}}_m, \boldsymbol{p})\\ &\quad = \boldsymbol{\varphi}_{c2}^{\mathrm{T}}(\boldsymbol{\theta}, \dot{\boldsymbol{\theta}}, \boldsymbol{p})\boldsymbol{\beta}_m + \boldsymbol{Y}_{c2}(\boldsymbol{\theta}, \dot{\boldsymbol{\theta}}, \boldsymbol{p})\end{aligned} \tag{40}$$

where $\boldsymbol{\varphi}_{c1}(\boldsymbol{\theta}, \dot{\boldsymbol{\theta}}, \dot{\boldsymbol{\theta}}_r, \ddot{\boldsymbol{\theta}}_r)$ is the corresponding regressor of β_r, $\boldsymbol{\varphi}_{c2}(\boldsymbol{\theta}, \dot{\boldsymbol{\theta}}, \boldsymbol{p})$ is the corresponding regressor of $\boldsymbol{\beta}_m$, $\boldsymbol{Y}_{c1}(\boldsymbol{\theta}, \dot{\boldsymbol{\theta}}, \dot{\boldsymbol{\theta}}_r, \ddot{\boldsymbol{\theta}}_r)$ and $\boldsymbol{Y}_{c2}(\boldsymbol{\theta}, \dot{\boldsymbol{\theta}}, \boldsymbol{p})$ are known nonlinear terms.

Merging (38), (39), (40), and (9), one obtains

$$\boldsymbol{M}\dot{\boldsymbol{z}}_2 + \boldsymbol{C}\boldsymbol{z}_2 = \boldsymbol{\tau} - \boldsymbol{\varphi}_{c1}^{\mathrm{T}}\beta_r - \boldsymbol{Y}_{c1} - \boldsymbol{\varphi}_{c2}^{\mathrm{T}}\boldsymbol{\beta}_m - \boldsymbol{Y}_{c2} - \tilde{\boldsymbol{d}}_t. \tag{41}$$

The desired virtual drive moment $\boldsymbol{\tau}_d$ is given by

$$\begin{aligned}\boldsymbol{\tau}_d &= \boldsymbol{\tau}_{da} + \boldsymbol{\tau}_{ds}\\ \boldsymbol{\tau}_{da} &= \boldsymbol{\tau}_{da1} + \boldsymbol{\tau}_{da2}\\ \boldsymbol{\tau}_{da1} &= \boldsymbol{\varphi}_{c1}^{\mathrm{T}}\hat{\beta}_r + \boldsymbol{\varphi}_{c2}^{\mathrm{T}}\hat{\boldsymbol{\beta}}_m + \boldsymbol{Y}_{c1} + \boldsymbol{Y}_{c2}\\ \boldsymbol{\tau}_{\mathrm{da2}} &= -\hat{\boldsymbol{d}}_{c1}\\ \boldsymbol{\tau}_{ds} &= \boldsymbol{\tau}_{ds1} + \boldsymbol{\tau}_{ds2}\\ \boldsymbol{\tau}_{ds1} &= -\boldsymbol{K}_2\boldsymbol{z}_2\end{aligned} \tag{42}$$

where $\boldsymbol{\tau}_{da1}$ represents the usual model compensation term with the physical parameter estimates $\hat{\boldsymbol{\beta}}_r$ and $\hat{\boldsymbol{\beta}}_m$ updated through the indirect type parameter estimation in the previous section, $\boldsymbol{\tau}_{da2}$ is the model compensation term with dynamic compensation type fast adaptation, $\hat{\boldsymbol{d}}_{c1}$ can be regarded as the estimate of the low frequency component of the lumped model uncertainties defined later, i.e., the lumped disturbance in task-space [12]–[14], $\boldsymbol{\tau}_{ds1}$ represents the robust feedback term with the positive definite control gain matrix $\boldsymbol{K}_2$, $\boldsymbol{\tau}_{\mathrm{ds2}}$ is synthesized later to dominate the model uncertainties coming from both parametric uncertainties and uncertain nonlinearities.

Then, the desired pressure vector can be obtained by (9)

$$\boldsymbol{p}_d = \boldsymbol{f}_t^{+}(\boldsymbol{\theta})[\boldsymbol{\tau}_d - \boldsymbol{g}_t(\boldsymbol{\theta})] + [\boldsymbol{I}_{3\times 3} - \boldsymbol{f}_t^{+}(\boldsymbol{\theta})\boldsymbol{f}_t(\boldsymbol{\theta})]\bar{\boldsymbol{p}}_0 \tag{43}$$

where $\bar{\boldsymbol{p}}_0$ is an arbitrary 3×1 vector related to the equivalent average stiffness [13] within permissible range of inner pressure of the pneumatic muscle, $\boldsymbol{f}_t^{+}(\boldsymbol{\theta})$ is the pseudo-inverse of $\boldsymbol{f}_t(\boldsymbol{\theta})$.

Let $\boldsymbol{z}_3 = \boldsymbol{p} - \boldsymbol{p}_d$ and substitute (42) and (43) into (41), then the dynamics of $\boldsymbol{z}_2$ is given by

$$\begin{aligned}\boldsymbol{M}\dot{\boldsymbol{z}}_2 + \boldsymbol{C}\boldsymbol{z}_2 &= \boldsymbol{M}(\ddot{\boldsymbol{\theta}} - \ddot{\boldsymbol{\theta}}_r) + \boldsymbol{C}(\dot{\boldsymbol{\theta}} - \dot{\boldsymbol{\theta}}_r)\\ &= -\boldsymbol{K}_2\boldsymbol{z}_2 + \boldsymbol{f}_t\boldsymbol{z}_3 + \boldsymbol{\varphi}_{c1}^{\mathrm{T}}\tilde{\boldsymbol{\beta}}_r\\ &\quad + \boldsymbol{\varphi}_{c2}^{\mathrm{T}}\tilde{\boldsymbol{\beta}}_m - \hat{\boldsymbol{d}}_{c1} - \tilde{\boldsymbol{d}}_t + \boldsymbol{\tau}_{ds2}.\end{aligned} \tag{44}$$

Define a constant vector $\boldsymbol{d}_{c1}$ and time-varying vector $\Delta_1(t)$ such that

$$\boldsymbol{d}_{c1} + \Delta_1 = \boldsymbol{\varphi}_{c1}^{\mathrm{T}}\tilde{\beta}_r + \boldsymbol{\varphi}_{c2}^{\mathrm{T}}\tilde{\boldsymbol{\beta}}_m - \tilde{\boldsymbol{d}}_t. \tag{45}$$

$\hat{\boldsymbol{d}}_{c1}$ is updated by the following projection type adaptation law [14]:

$$\dot{\hat{\boldsymbol{d}}}_{c1} = \mathrm{Proj}_{\hat{\boldsymbol{d}}_{c1}}(\gamma_{d1}\boldsymbol{z}_2) = \begin{cases} 0, & \text{if } \left|\hat{\boldsymbol{d}}_{c1}(t)\right| = \boldsymbol{d}_{c1M} \text{ and } \hat{\boldsymbol{d}}_{c1}(t)\boldsymbol{z}_2 > 0 \\ \gamma_{d1}\boldsymbol{z}_2, & \text{else} \end{cases} \quad (46)$$

with $\gamma_{\mathrm{d1}} > 0$, $\left|\hat{\boldsymbol{d}}_{c1}(0)\right| \le \boldsymbol{d}_{c1M}$ in which $\boldsymbol{d}_{c1M}$ is a preset bound and larger than zero.

$\boldsymbol{\tau}_{ds2}$ is chosen to satisfy the following conditions:

$$\begin{cases} \boldsymbol{z}_2^{\mathrm{T}}\left(\boldsymbol{\tau}_{ds2} + \Delta_1 - \tilde{\boldsymbol{d}}_{\mathrm{c1}}\right) \le \varepsilon_2 \\ \boldsymbol{z}_2^{\mathrm{T}}\boldsymbol{\tau}_{ds2} \le 0 \end{cases} \quad (47)$$

where ε_2 is a positive design parameter that may be arbitrarily small. For example, $\boldsymbol{\tau}_{ds2}$ may be chosen as [27]

$$\boldsymbol{\tau}_{ds2} = -\boldsymbol{K}_{2s}\tanh\left(\frac{\boldsymbol{z}_2}{\varepsilon_2}\right) \quad (48)$$

where $\boldsymbol{K}_{2s}$ is a positive definite diagonal matrix decided by uncertain nonlinearities in task-space.

Define the positive semi-definite (p.s.d) function as

$$V_2 = \frac{1}{2}\boldsymbol{z}_2^{\mathrm{T}}\boldsymbol{M}\boldsymbol{z}_2. \quad (49)$$

Differentiate V_2 and substitute (44)–(47) into it, one obtains

$$\begin{aligned} \dot{V}_2 &= -\boldsymbol{z}_2^{\mathrm{T}}\boldsymbol{K}_2\boldsymbol{z}_2 + \boldsymbol{z}_2^{\mathrm{T}}\boldsymbol{f}_t\boldsymbol{z}_3 + \boldsymbol{z}_2^{\mathrm{T}}[\boldsymbol{\tau}_{\mathrm{ds2}} + \Delta_1 - \tilde{\boldsymbol{d}}_{\mathrm{c1}}] \\ &\le -\boldsymbol{z}_2^{\mathrm{T}}\boldsymbol{K}_2\boldsymbol{z}_2 + \boldsymbol{z}_2^{\mathrm{T}}\boldsymbol{f}_t\boldsymbol{z}_3 + \varepsilon_2. \end{aligned} \quad (50)$$

As can be seen from (50), if $\boldsymbol{z}_3$ is bounded, $\boldsymbol{z}_2$ would be bounded.

Step 2: Next is to synthesize an average flow rate $\boldsymbol{q}_m$ so that $\boldsymbol{z}_3$ would converge to zero or a small value with a guaranteed transient performance.

While noting the dynamics of actuator in (9), the time derivative of $\boldsymbol{z}_3$ is

$$\dot{\boldsymbol{z}}_3 = \dot{\boldsymbol{p}} - \dot{\boldsymbol{p}}_d = \boldsymbol{f}_p\boldsymbol{q}_m + \boldsymbol{g}_p + \boldsymbol{d}_p - \dot{\boldsymbol{p}}_{\mathrm{dc}} - \dot{\boldsymbol{p}}_{\mathrm{du}} \quad (51)$$

where $\dot{\boldsymbol{p}}_{\mathrm{dc}} = \partial\boldsymbol{p}_d/\partial t + \partial\boldsymbol{p}_d/\partial\boldsymbol{\theta}\dot{\hat{\boldsymbol{\theta}}} + \partial\boldsymbol{p}_{\mathrm{d}}/\partial\dot{\boldsymbol{\theta}}\ddot{\hat{\boldsymbol{\theta}}} + \partial\boldsymbol{p}_d/\partial\hat{\beta}_t\dot{\hat{\boldsymbol{\beta}}}_t$, $\dot{\boldsymbol{p}}_{\mathrm{du}} = \partial\boldsymbol{p}_d/\partial\boldsymbol{\theta}\left(\dot{\boldsymbol{\theta}} - \dot{\hat{\boldsymbol{\theta}}}\right) + \partial\boldsymbol{p}_d/\partial\dot{\boldsymbol{\theta}}\left(\ddot{\boldsymbol{\theta}} - \ddot{\hat{\boldsymbol{\theta}}}\right)$ in which $\dot{\hat{\boldsymbol{\theta}}}$ and $\ddot{\hat{\boldsymbol{\theta}}}$ are obtained from $\boldsymbol{\theta}$ by a second-order differential filter as in [11], $\dot{\boldsymbol{p}}_{\mathrm{dc}}$ represents the calculable part of $\dot{\boldsymbol{p}}_d$ and can be used to design control functions, but $\dot{\boldsymbol{p}}_{\mathrm{du}}$ cannot due to various uncertainties.

The desired average flow rate $\boldsymbol{q}_{md}$ is designed as

$$\begin{aligned} \boldsymbol{q}_{md} &= \boldsymbol{q}_{mda} + \boldsymbol{q}_{mds} \\ \boldsymbol{q}_{mda} &= \boldsymbol{q}_{mda1} + \boldsymbol{q}_{mda2} \\ \boldsymbol{q}_{mda1} &= \hat{\boldsymbol{f}}_p^{-1}\left(-\boldsymbol{f}_t^{\mathrm{T}}\boldsymbol{z}_2 - \hat{\boldsymbol{g}}_{\mathrm{p}} - \hat{\boldsymbol{d}}_{\mathrm{p0}} + \dot{\boldsymbol{p}}_{\mathrm{dc}}\right) \\ \boldsymbol{q}_{mda2} &= -\hat{\boldsymbol{f}}_p^{-1}\hat{\boldsymbol{d}}_{c2} \\ \boldsymbol{q}_{mds} &= \boldsymbol{q}_{mds1} + \boldsymbol{q}_{mds2} \\ \boldsymbol{q}_{mds1} &= -\hat{\boldsymbol{f}}_p^{-1}\boldsymbol{K}_3\boldsymbol{z}_3 \end{aligned} \quad (52)$$

where $\boldsymbol{q}_{mda1}$ represents the usual model compensation with $\hat{\boldsymbol{f}}_p$, $\hat{\boldsymbol{g}}_p$ and $\hat{\boldsymbol{d}}_{p0}$, which are calculated by the physical parameter estimates $\hat{\boldsymbol{\beta}}_p$ updated through the indirect type parameter estimation in the previous section, $\boldsymbol{q}_{mda2}$ is the model compensation term with the dynamic compensation type fast adaptation, $\hat{\boldsymbol{d}}_{c2}$ can be regarded as the estimate of the low frequency component of the lumped model uncertainties defined later, i.e., lumped disturbance in muscle-space, $\boldsymbol{q}_{mds1}$ represents the robust feedback term with the positive definite control gain matrix $\boldsymbol{K}_3$, $\boldsymbol{q}_{mds2}$ is synthesized later to dominate the model uncertainties.

Substitute (52) into (51), then the dynamics of $\boldsymbol{z}_3$ is

$$\begin{aligned} \dot{\boldsymbol{z}}_3 = &-\boldsymbol{K}_3\boldsymbol{z}_3 - \hat{\boldsymbol{d}}_{c2} - \tilde{\boldsymbol{f}}_p\boldsymbol{q}_{md} - \tilde{\boldsymbol{g}}_p \\ &- \tilde{\boldsymbol{d}}_{p0} + \tilde{\boldsymbol{d}}_p - \dot{\boldsymbol{p}}_{du} + \hat{\boldsymbol{f}}_p\boldsymbol{q}_{mds2}. \end{aligned} \quad (53)$$

Define a constant vector $\boldsymbol{d}_{c2}$ and time-varying vector $\Delta_2(t)$ such that

$$\boldsymbol{d}_{c2} + \Delta_2 = -\tilde{\boldsymbol{f}}_p\boldsymbol{q}_{md} - \tilde{\boldsymbol{g}}_p - \tilde{\boldsymbol{d}}_{p0} + \tilde{\boldsymbol{d}}_p - \dot{\boldsymbol{p}}_{du}. \quad (54)$$

$\hat{\boldsymbol{d}}_{c2}$ is updated by the following projection type adaptation law [14]:

$$\dot{\hat{\boldsymbol{d}}}_{c2} = \mathrm{Proj}_{\hat{\boldsymbol{d}}_{c2}}(\gamma_{d2}\boldsymbol{z}_3) = \begin{cases} 0, & \text{if } \left|\hat{\boldsymbol{d}}_{c2}(t)\right| = \boldsymbol{d}_{c2M} \text{ and } \hat{\boldsymbol{d}}_{c2}(t)\boldsymbol{z}_3 > 0 \\ \gamma_{\mathrm{d2}}\boldsymbol{z}_3, & \text{else} \end{cases} \quad (55)$$

with $\gamma_{d2} > 0$, $\left|\hat{\boldsymbol{d}}_{c2}(0)\right| \le \boldsymbol{d}_{c2M}$ in which $\boldsymbol{d}_{c2M}$ is a preset bound and larger than zero.

$\boldsymbol{q}_{mds2}$ is chosen to satisfy the following conditions:

$$\begin{cases} \boldsymbol{z}_3^{\mathrm{T}}(\hat{\boldsymbol{f}}_p\boldsymbol{q}_{mds2} + \Delta_2 - \tilde{\boldsymbol{d}}_{c2}) \le \varepsilon_3 \\ \boldsymbol{z}_3^{\mathrm{T}}\hat{\boldsymbol{f}}_p\boldsymbol{q}_{mds2} \le 0 \end{cases} \quad (56)$$

where ε_3 is a positive design parameter that may be arbitrarily small. For example, $\boldsymbol{q}_{mds2}$ may be chosen as [27]

$$\boldsymbol{q}_{mds2} = -\boldsymbol{K}_{3s}\tanh\left(\frac{\boldsymbol{z}_3}{\varepsilon_3}\right) \quad (57)$$

where $\boldsymbol{K}_{3s}$ is a positive definite diagonal matrix decided by uncertain nonlinearities.

To see how the above control function works, define a p.s.d. function as

$$V_3 = V_2 + \frac{1}{2}\boldsymbol{z}_3^{\mathrm{T}}\boldsymbol{z}_3. \quad (58)$$

Differentiate V_3 and substitute (50), (53) and (54) into it, one obtains

$$\begin{aligned} \dot{V}_3 = &-\boldsymbol{z}_2^{\mathrm{T}}\boldsymbol{K}_2\boldsymbol{z}_2 - \boldsymbol{z}_3^{\mathrm{T}}\boldsymbol{K}_3\boldsymbol{z}_3 + \boldsymbol{z}_2^{\mathrm{T}}(\boldsymbol{\tau}_{ds2} + \Delta_1 - \tilde{\boldsymbol{d}}_{c1}) \\ &+ \boldsymbol{z}_3^{\mathrm{T}}(\hat{\boldsymbol{f}}_p\boldsymbol{q}_{mds2} + \Delta_2 - \tilde{\boldsymbol{d}}_{c2}). \end{aligned} \quad (59)$$

Substitute (47) and (56) into (59), $\dot{V}_3$ is bounded above by the following equation:

$$\dot{V}_3 \le -\boldsymbol{z}_2^{\mathrm{T}}\boldsymbol{K}_2\boldsymbol{z}_2 - \boldsymbol{z}_3^{\mathrm{T}}\boldsymbol{K}_3\boldsymbol{z}_3 + \varepsilon_2 + \varepsilon_3. \quad (60)$$

Step 3: As for the PMDPM controlled by fast switching valves, the valve dynamics is neglected since the dynamic response of the valve is much higher than that of the mechanical system. Then, the inverse flow mappings are used to calculate the specific duty cycle commands of the fast switching valves for providing the desired average flow rates $\boldsymbol{q}_{md}$. The control input vector is given by

$$\boldsymbol{u} = \boldsymbol{K}_q^{-1}\boldsymbol{q}_{md}. \tag{61}$$

B. Supplementary Specification

With the previously mentioned controller design, the following theoretical results on the performance of the proposed integrated DIARC for the PMDPM can be obtained.

Theorem 1: Considering the control law (61) with the rate limited projection type adaptation law (29) and (35), in general, all signals of the resulting closed-loop system are bounded. In addition, the output tracking error $\boldsymbol{z} = \left[\boldsymbol{z}_2^{\mathrm{T}}, \boldsymbol{z}_3^{\mathrm{T}}\right]^{\mathrm{T}}$ is bounded above by

$$\|\boldsymbol{z}(t)\|^2 \leq \exp(-\lambda_v t)\,\|\boldsymbol{z}(0)\| + \frac{2\varepsilon_v}{\lambda_v}[1-\exp(-\lambda_v t)] \tag{62}$$

where $\lambda_v = 2 \times \min(\boldsymbol{K}_2, \boldsymbol{K}_3)$, $\varepsilon_v = \varepsilon_2 + \varepsilon_3$.

Proof: As the boundedness of the parameter estimates $\hat{\boldsymbol{\beta}}$ and $\dot{\hat{\boldsymbol{\beta}}}$ are guaranteed by P1 and P3, respectively, one can follow the above standard backstepping design procedure to show that all the control functions (42), (43), and (52) and states $\boldsymbol{\theta}$, $\dot{\boldsymbol{\theta}}$, $\boldsymbol{p}$ are bounded for any bounded desired trajectory with bounded higher derivatives. Therefore, all signals of the closed-loop system are bounded [14] and (60) leads to (62) by using the Comparison Lemma [28]. Thus, the proof of the theorem is completed.

Remark 1: For the parallel manipulator, the physical regression model (19) is integrated with two additional regression models (22) and (23) to improve the effective convergence of parameter estimation by choosing appropriate weights in the composite error minimizing criterion. Thus, the reliable and optimal estimates of effective model parameters are obtained to decrease the parametric uncertainties in (19) and achieve small tracking errors consequently.

Remark 2: The weights ω_1, ω_2, and ω_3 in the composite error minimizing criterion (24) have significant effects on the performance of parameter estimation.

a) ω_1 influences the prediction error of physical dynamics. Larger magnitude of ω_1 contributes to smaller prediction error, while brings much larger covariance of parameter estimations and may lead to worse performance.
b) ω_2 affects the extent of $\Delta\boldsymbol{F}_{m0}$. Larger ω_2 leads to smaller $\Delta\boldsymbol{F}_{m0}$ and obtains more reasonable parameter estimates since theoretical static forces are consistent with the physical characteristics of pneumatic muscles and reasonable in practice.
c) ω_3 influences the extent of $\Delta\boldsymbol{A}$ that determines the neglected uncertain nonlinearities coming from the time derivative of $\boldsymbol{p}$ when calculating the time derivative of $\boldsymbol{p}_d$ in controller design. Larger ω_3 will contribute to smaller uncertain nonlinearities neglected by controller design.

Remark 3: For effective convergence of parameter estimation, the physical parameter estimation is conducted only when the following persistent-exciting-like condition is satisfied, which can be deduced from (27), (28), and (30) with $\alpha_1 = \alpha_2 = \alpha_3 = \alpha_4$

$$\int_t^{t+T} \left(\omega_1\boldsymbol{\varphi}_1\boldsymbol{\varphi}_1^{\mathrm{T}} + \omega_2\boldsymbol{\varphi}_2\boldsymbol{\varphi}_2^{\mathrm{T}} + \omega_3\boldsymbol{\varphi}_3\boldsymbol{\varphi}_3^{\mathrm{T}}\right) dt \geq k_p\boldsymbol{I}_p, \quad k_p > 0 \tag{63}$$

where $T > 0$.

V. Experimental Results

The proposed integrated DIARC, which the new parameter estimation algorithm based on composite error minimizing criterion is applied into, is implemented on the parallel manipulator driven by pneumatic muscles (PMDPM).

A. Experimental Settings

The precision of position transducer is within 0.06 mm, which is currently limited by the resolution of A/D acquisition, thus the calculated posture precision is about 0.01°. The supply pressure is set at 0.5MPa. The initial theoretical contractive force of pneumatic muscle is set according to the technique data from Festo [29]. The offline estimated contractive forces of pneumatic muscles are regarded as the theoretical contractive forces, and then the online parameter estimation algorithm is used to reduce model errors of contractive forces and further improve control accuracy. The integrated DIARC and the DARC [12] would be compared in experiments. Note that the DARC has the same design procedure as the integrated DIARC except that the parameter estimation of the DARC is based on tracking error dynamics as opposed to physical dynamics in the integrated DIARC.

As can be seen from (62), smaller magnitudes of ε_2 and ε_3 and larger magnitudes of $\boldsymbol{K}_c$, $\boldsymbol{K}_2$, $\boldsymbol{K}_3$, $\boldsymbol{K}_{2s}$, $\boldsymbol{K}_{3s}$ should be chosen for faster converging rate and smaller tracking errors. However, they are all constrained by the achievable bandwidth of the closed-loop system. Thus, the control parameters of the two controllers are as follows.

In the integrated DIARC, the feedback gains are $\boldsymbol{K}_1 = \mathrm{diag}([80,80]^{\mathrm{T}})$, $\boldsymbol{K}_2 = \mathrm{diag}([30,30]^{\mathrm{T}})$, $\boldsymbol{K}_3 = \mathrm{diag}([5,5,5]^{\mathrm{T}})$, $\boldsymbol{K}_{2s} = \mathrm{diag}([0.5,0.5]^{\mathrm{T}})$, $\boldsymbol{K}_{3s} = \mathrm{diag}([20000,20000,20000]^{\mathrm{T}})$. The online estimated parameters are $\boldsymbol{\beta}_t = [\boldsymbol{d}_{t0}^{\mathrm{T}}, a_1, a_2, b_1, b_2, a_{f1}, a_{f2}]^{\mathrm{T}}$ with the initial values being $\boldsymbol{\beta}_t(0) = [0,0,0,0,0,0,0,0]^{\mathrm{T}}$, and the rest parameters are fixed to their offline estimates. The adaptation gain matrices are $\gamma_{d2} = \mathrm{diag}([70,70]^{\mathrm{T}}$, $\boldsymbol{\gamma}_{d3} = \mathrm{diag}([5,5,5]^{\mathrm{T}})$, $\boldsymbol{\gamma}_1(0) = \mathrm{diag}([1e4,1e4,1e4,1e4,1e4,1e4,1e4,1e4]^{\mathrm{T}})$. Other parameters are $\varepsilon_2 = 0.03$, $\varepsilon_3 = 2000$, $\omega_1 = 1$, $\omega_2 = 0.0002$, $\omega_3 = 2.5e6$.

In the DARC, the feedback gains $\boldsymbol{K}_1$, $\boldsymbol{K}_2$, $\boldsymbol{K}_3$, $\boldsymbol{K}_{2s}$, $\boldsymbol{K}_{3s}$, ε_2, ε_3, and adaptation gain matrices $\boldsymbol{\gamma}_{d2}$, $\boldsymbol{\gamma}_{d3}$ are the same as those in the integrated DIARC. The adaptation gain matrix is $\boldsymbol{\gamma}_1 = \mathrm{diag}([0.01,0.001,0.01,0.001,0.001,0.001]^{\mathrm{T}})$.

B. Sinusoidal Trajectory Tracking

For tracking a sinusoidal trajectory (amplitude $\theta_x = 3°$, $\theta_y = 5°$, and period 15 s), response comparison between the

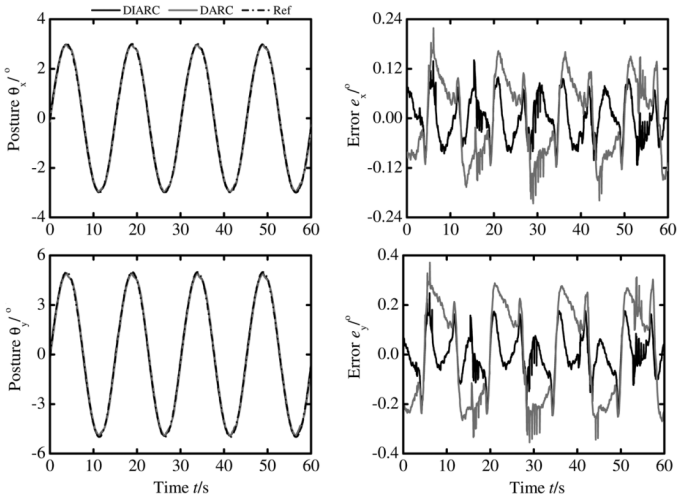

Fig. 2. Tracking responses of sinusoidal trajectory (period = 15 s) with the integrated DIARC and the DARC.

TABLE I
PERFORMANCE COMPARISON BETWEEN THE INTEGRATED DIARC AND THE DARC UNDER SINUSOIDAL TRAJECTORY TRACKING

Performance	Integrated DIARC	DARC
$L_2[e](\theta_x, \theta_y)$	$[0.0514, 0.0842]$	$[0.0922, 0.1981]$
$e_M(\theta_x, \theta_y)$	$[0.1406, 0.2477]$	$[0.2181, 0.3714]$
$e_F(\theta_x, \theta_y)$	$[0.1133, 0.2215]$	$[0.1499, 0.3113]$
$L_2[u](u_1, u_2, u_3)$	$[0.2396, 0.2299, 0.5508]$	$[0.2374, 0.2292, 0.5276]$
$c_u(u_1, u_2, u_3)$	$[0.0809, 0.0780, 0.0667]$	$[0.0814, 0.0806, 0.0748]$

integrated DIARC and the DARC is shown in Fig. 2, and the performance comparison between the two controllers is shown in Table I wherein the performance indexes are defined in [30]. In the following figures, e_x and e_y represent the tracking errors of posture along x-axis and y-axis, respectively. d_{p1}, d_{p2}, and d_{p3} represent the lumped disturbances in muscle-space. $d_{\rm tx}$ and $d_{\rm ty}$ represent the lumped disturbances in task-space along x-axis and y-axis, respectively. As can be seen from Fig. 2 and Table I, the final tracking errors and the average tracking errors with the integrated DIARC are much smaller than those with the DARC as expected.

To illustrate the effectiveness of the new parameter estimation algorithm based on composite error minimizing criterion, lumped disturbance estimates, and physical parameter estimates with the integrated DIARC and the DARC under the sinusoidal trajectory tracking are respectively shown in Figs. 3–5. Since the estimation algorithms in the DARC are of gradient type and there are too many unknown parameters to be adapted, the parameter estimates may be unreasonable resulting in saturation of control inputs and further leading to fluctuations of the PMDPM when the adaptation rate matrix of physical parameters is inappropriate. In order to avoid fluctuations, the adaptation rate matrix of physical parameters used in the DARC is usually very small and then parametric uncertainties are mainly compensated by lumped disturbance estimates rather than the poor physical parameter estimates. In contrast with the integrated DIARC, average tracking errors and maximum tracking errors under the control of the DARC are a little larger.

Under certain theoretical contractive forces of pneumatic muscles, parametric uncertainties are almost compensated with

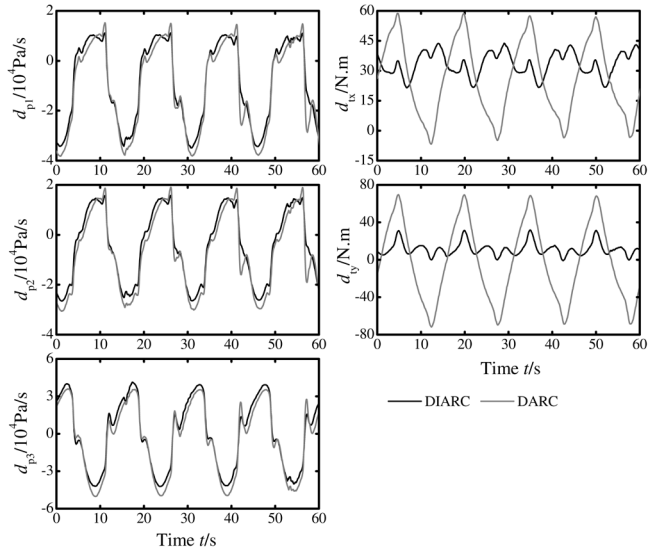

Fig. 3. Lumped disturbance estimates in task-space and muscle-space with the integrated DIARC and the DARC under the sinusoidal trajectory tracking.

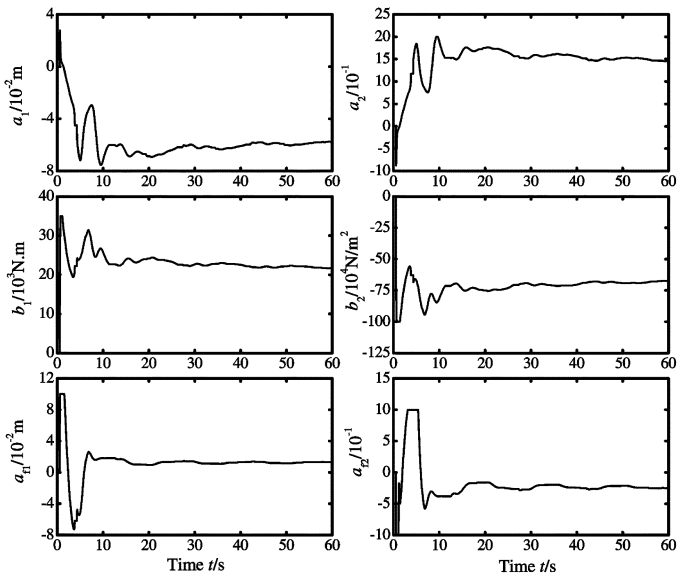

Fig. 4. Physical parameter estimates in task-space with the integrated DIARC under the sinusoidal trajectory tracking.

the integrated DIARC owing to the reliable and effective parameter estimations. Therefore, the lumped uncertain nonlinearities of the parallel manipulator, i.e., the lumped disturbances in task-space, are fairly small and then the final tracking errors and average tracking errors are small as well. It is noted that the added constraints related to the known theoretical contractive forces in the parameter estimation of the integrated DIARC would reshape the regression model to improve the parameter estimation significantly and then lead to excellent performance consequently.

To further test the achievable control performance of the proposed integrated DIARC, fast switching valves with larger flow rates (MHE4-MS1H-3/2-G-QS8K by Festo) are used for tracking a faster sinusoidal trajectory (amplitude $\theta_x = 3°$, $\theta_y = 5°$, and period 5 s). As can be seen from Fig. 6, the final tracking errors with the integrated DIARC are

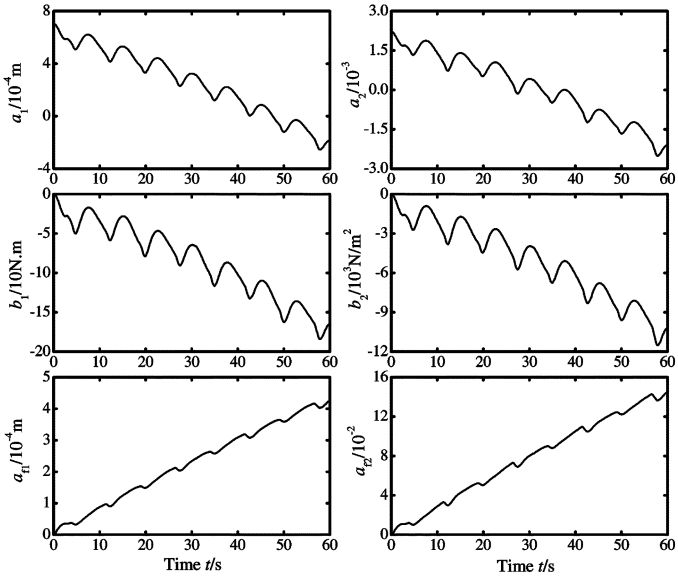

Fig. 5. Physical parameter estimates in task-space with the DARC under the sinusoidal trajectory tracking.

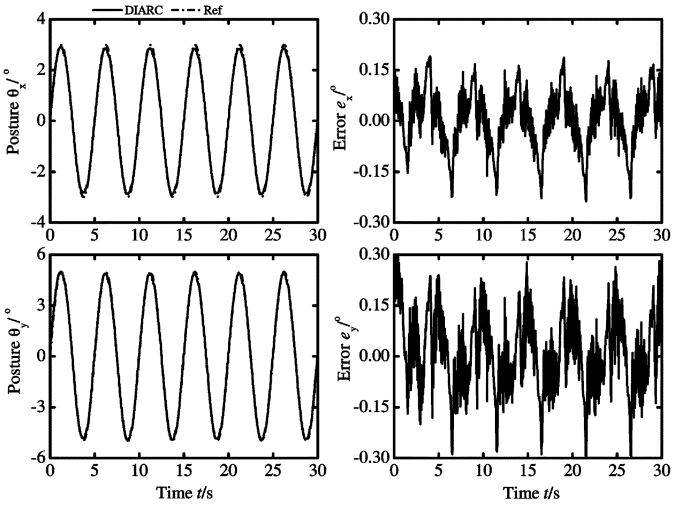

Fig. 6. Tracking responses of the sinusoidal trajectory (period = 5 s) with the integrated DIARC.

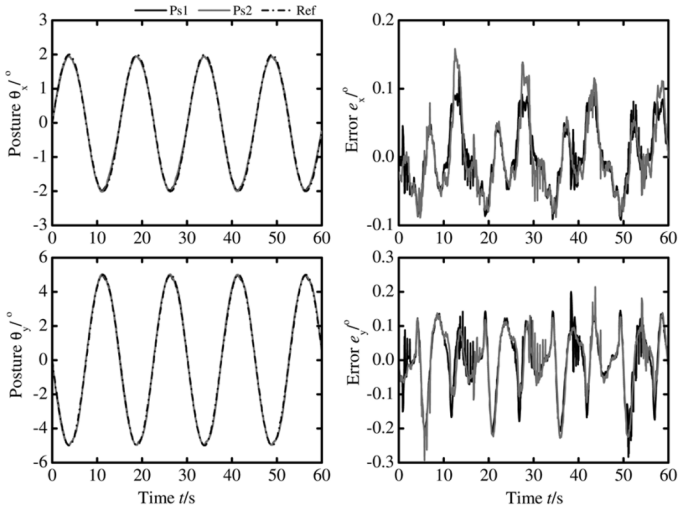

Fig. 7. Tracking responses of the sinusoidal trajectory with the integrated DIARC under different supply pressures.

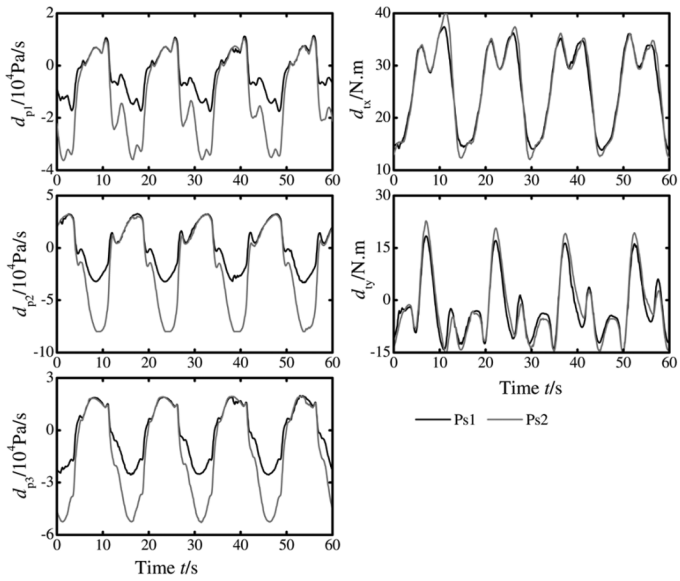

Fig. 8. Lumped disturbance estimates in task-space and muscle-space with the integrated DIARC under different supply pressures.

$e_{Fx} = 0.2261°$, $e_{Fy} = 0.2897°$, and the average tracking errors are $L_2[e_x] = 0.0863°$, $L_2[e_y] = 0.1213°$, the performance is almost equivalent to that of Fig. 2.

C. Robustness Tests Under Different Supply Pressures and Sudden Disturbance

To test the influence of uncertainties in the nonlinear flow gain on the control performance, sinusoidal trajectory tracking with the integrated DIARC is conducted under different supply pressures (see Fig. 7), and the performance index comparison between $P_{s1} = 0.5$ MPa and $P_{s2} = 0.39$ MPa is shown in Table II. Lumped disturbance estimates in task-space and muscle-space with the integrated DIARC are shown in Fig. 8 and control inputs are shown in Fig. 9. Obviously, the control inputs under different supply pressures vary a little (see Fig. 9), but tracking errors under different supply pressures vary slightly (see Fig. 7 and Table II), as lumped disturbances in muscle-space are effectively compensated by parameter estimation regardless of supply pressure variations (see Fig. 8).

Tracking response of a smooth step trajectory being initialized is shown in Fig. 10. As can be seen, the steady-state errors are $e_{Fx} = 0.00645°$, $e_{Fy} = 0.01080°$. Simultaneously, for testing the robustness of the integrated DIARC suffering from a sudden disturbance, one position transducer is given a sudden dither at $t = 55$ s, which can be regarded as a sudden large disturbance to the PMDPM. The PMDPM experiences large tracking errors due to the wrong feedback information of the position transducer when the dither is introduced. But after the dither disappeared, the PMDPM comes back to the stable posture quickly with no fluctuation. This demonstrates the robustness of the proposed control algorithm to disturbances.

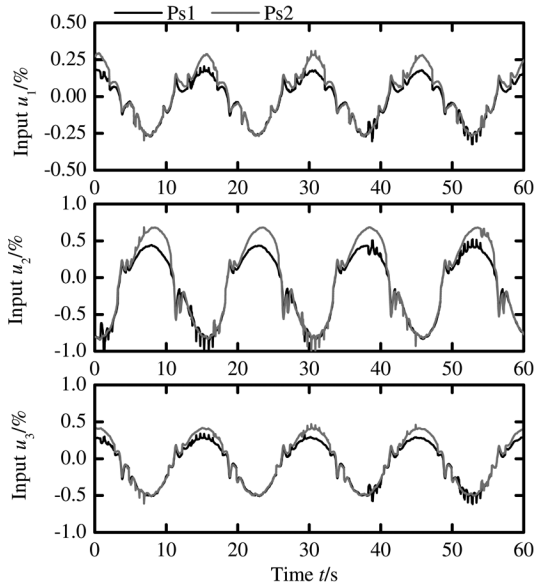

Fig. 9. Control inputs with the integrated DIARC under different supply pressures.

TABLE II
PERFORMANCE COMPARISON BETWEEN DIFFERENT SUPPLY PRESSURES WITH THE INTEGRATED DIARC

Performance	$P_{s1} = 0.5$MPa	$P_{s2} = 0.39$MPa
$L_2[e](\theta_x, \theta_y)$	$[0.0461, 0.0872]$	$[0.0529, 0.0875]$
$e_M(\theta_x, \theta_y)$	$[0.1272, 0.2837]$	$[0.1581, 0.2931]$
$e_F(\theta_x, \theta_y)$	$[0.0950, 0.2837]$	$[0.1155, 0.2249]$
$L_2[u](u_1, u_2, u_3)$	$[0.1412, 0.4754, 0.285]$	$[0.1700, 0.5437, 0.325]$
$c_u(u_1, u_2, u_3)$	$[0.0985, 0.0746, 0.082]$	$[0.0800, 0.0715, 0.068]$

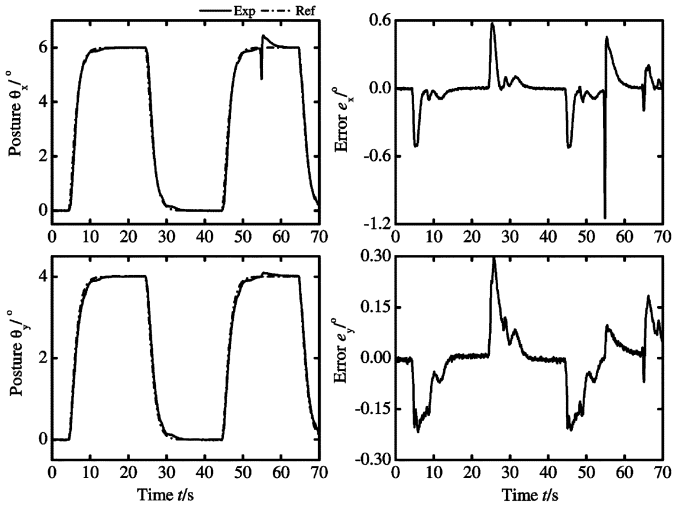

Fig. 10. Smooth step response and robustness test under a sudden disturbance.

D. Estimating Capability for Time-Varying Trajectory

Tracking response of a time-varying sinusoidal trajectory with the integrated DIARC is shown in Fig. 11. The trajectory varies from $\theta_x = 3\sin(2\pi t/15)$ and $\theta_y = -6\sin(2\pi t/15)$ to $\theta_x = 6\sin(2\pi t/15)$ and $\theta_y = 1\sin(2\pi t/15)$ at $t = 45$ s. As can be seen, transient tracking errors vary slightly in the process of tracking two sinusoidal trajectories and the maximum tracking errors are $e_{Mx} = 0.41963°$ and $e_{My} = 0.38927°$ and occur

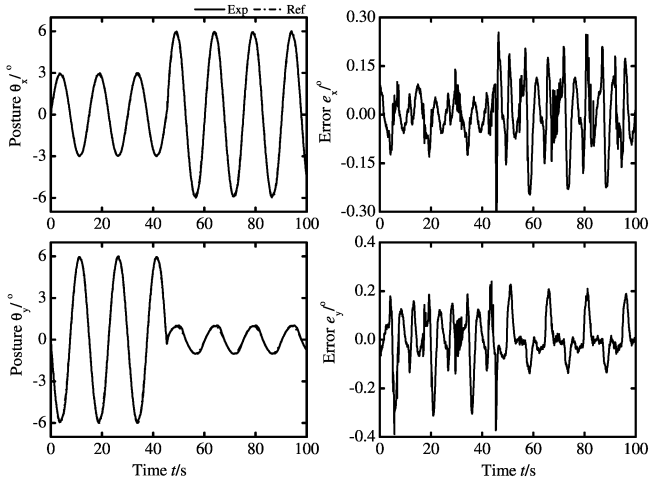

Fig. 11. Tracking response of the time-varying sinusoidal trajectory with the integrated DIARC.

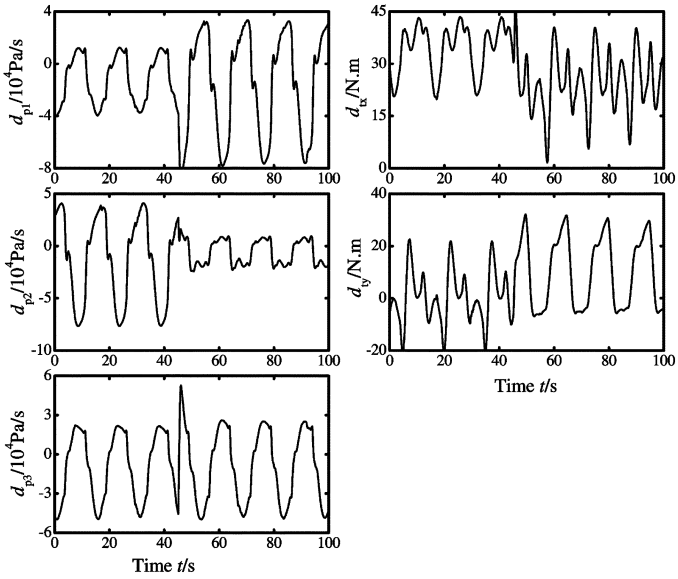

Fig. 12. Lumped disturbance estimates in task-space and muscle-space with the integrated DIARC under the time-varying sinusoidal trajectory tracking.

at the turning point. To further illustrate estimating capability of the integrated DIARC for tracking the time-varying trajectory, lumped disturbance estimates and physical parameter estimates under the time-varying sinusoidal trajectory tracking are, respectively, shown in Figs. 12 and 13. Obviously, once the reference trajectories vary, the parameter estimation will obtain new optimal values of parameters to make model errors as small as possible and finally achieve small tracking errors again. At the same time, lumped disturbance estimates will quickly adapt to the variation of the trajectories in order to compensate large uncertainties. Thus, with the effort of physical parameter estimation and lumped disturbance estimation, the tracking errors will keep small all the time.

VI. CONCLUSION

On the basis of reliable and effective parameter estimation, an integrated DIARC is synthesized for achieving high preci-

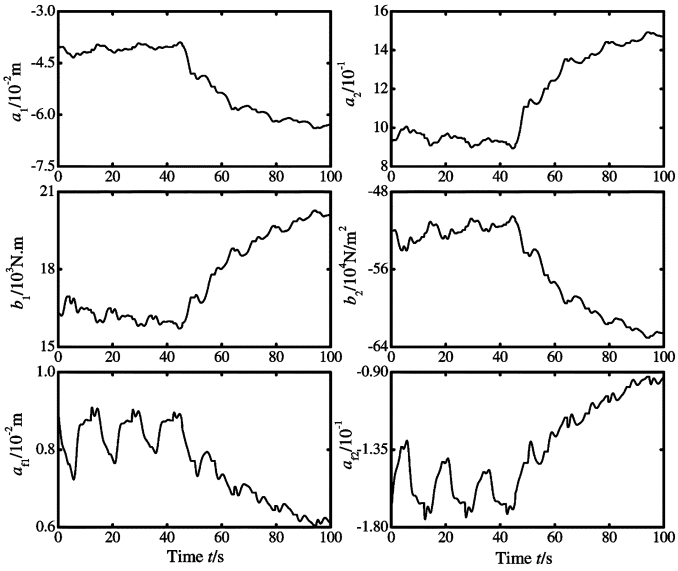

Fig. 13. Physical parameter estimates in task-space with the integrated DIARC under the time-varying sinusoidal trajectory tracking.

sion posture trajectory tracking control of the PMDPM. The integrated DIARC utilizes the indirect type parameter estimation that compensates the parametric uncertainties for reducing large transient tracking errors, and employs the dynamic compensation type fast adaptation that further attenuates the extent of uncertain nonlinearities for better tracking performance. Therein, a new parameter estimation algorithm based on composite error minimizing criterion is proposed for the parallel manipulator to overcome the poor parameter estimation of the conventional parameter estimation algorithm based on single error minimizing criterion, which is caused by the difficulty in satisfying the persistent exciting conditions all the time.

It is proved by experimental results that the integrated DIARC achieves excellent tracking performance with the maximum tracking error less than 0.3° and the average tracking error less than 0.1° and the steady-state error less than 0.01°, which are much smaller than those with the DARC. Moreover, the controller is robust to different supply pressures and sudden disturbances and could achieve effective parameter estimation regardless of time-varying reference trajectories.

ACKNOWLEDGMENT

The authors would like to thank the Festo(China) Ltd. for donating pneumatic components used in experiments.

REFERENCES

[1] S. Hesse, *The Fluidic Muscle in Application*. Germany: Festo AG & Co. KG, 2003.

[2] B. Tondu and P. Lopez, "Modeling and control of McKibben artificial muscle robot actuators," *IEEE Control Syst. Mag.*, vol. 20, no. 2–38, p. 15, Apr. 2000.

[3] P. Carbonell, Z. P. Jiang, and D. W. Repperger, "Nonlinear control of a pneumatic muscle actuator: backstepping vs. sliding-mode," in *Proc. IEEE Conf. Control Appl.*, Mexico City, Mexico, Sep. 2001, pp. 167–172.

[4] A. Hildebrandt, O. Sawodny, R. Neumann, and A. Hartmann, "Cascaded control concept of a robot with two degrees of freedom driven by four artificial pneumatic muscle actuators," in *Proc. Amer. Control Conf.*, Portland, OR, Jun. 2005, pp. 680–685.

[5] A. Hildebrandt, O. Sawodny, R. Neumann, and A. Hartmann, "A flatness based design for tracking control of pneumatic muscle actuators," in *Proc. 7th Int. Conf. Control, Autom., Robot. Vision (ICARCV)*, Singapore, Dec. 2002, pp. 1156–1161.

[6] N. G. Tsagarakis and D. G. Caldwell, "Development and control of a 'soft-actuated' exoskeleton for use in physiotherapy and training," *Autonomous Robots*, vol. 15, no. 1, pp. 21–33, Jul. 2003.

[7] K. Kawashima, N. Nakamura, T. Miyata, and T. Kagawa, "Application of robots using pneumatic artificial rubber muscles for operating construction machines," in *Proc. IEEE/RSJ Int. Conf. Intell. Robots Syst.*, Las Vegas, NE, Oct. 2003, pp. 3384–3389.

[8] G. K. Klute, J. M. Czerniecki, and B. Hannaford, "McKibben artificial muscles: pneumatic actuators with biomechanical intelligence," in *Proc. IEEE/ASME Int. Conf. Adv. Intell. Mechatron.*, Atlanta, GA, Sep. 1999, pp. 221–226.

[9] G. L. Tao, X. C. Zhu, and J. Cao, "Modeling and controlling of parallel manipulator joint driven by pneumatic muscles," *Chinese J. Mechan. Eng. (English Ed.)*, vol. 18, no. 4, pp. 537–541, Dec. 2005.

[10] X. C. Zhu and G. L. Tao, "Modeling of a servo platform driven by pneumatic artificial muscles," *J. Zhejiang Univ. (Eng. Sci.)*, vol. 38, no. 8, pp. 1056–1060, Aug. 2004.

[11] X. C. Zhu, G. L. Tao, J. Cao, and B. Yao, "Adaptive robust posture control of a pneumatic muscles driven parallel manipulator," in *Proc. 4th IFAC Symp. Mechatron. Syst.*, Heidelberg, Germany, Sep. 2006, pp. 764–769.

[12] X. C. Zhu, G. L. Tao, B. Yao, and J. Cao, "Adaptive robust posture control of a parallel manipulator driven by pneumatic muscles," *Automatica*, vol. 44, no. 9, pp. 2248–2257, Sep. 2008.

[13] G. L. Tao, X. C. Zhu, B. Yao, and J. Cao, "Adaptive robust posture control of a pneumatic muscles driven parallel manipulator with redundancy," in *Proc. Amer. Control Conf.*, New York City, Jul. 2007, pp. 3408–3413.

[14] B. Yao, "Integrated direct/indirect adaptive robust control of SISO nonlinear systems in semi-strict feedback form," in *Proc. Amer. Control Conf.*, Denver, CO, Jun. 2003, pp. 3020–3025.

[15] J. H. Zhang, *Parameter Estimation and Its Improvement of Linear Model*, 2nd ed. Changsha, China: National University of Defence Technology Press, 1999.

[16] X. C. Zhu, G. L. Tao, and J. Cao, "Parametric identification of a parallel manipulator with redundancy driven by pneumatic muscles," *Chinese J. Mechan. Eng. (English Ed.)*, vol. 21, no. 1, pp. 66–71, Feb. 2008.

[17] T. Kerscher, J. Albiez, J. M. Zollner, and R. Dillmann, "Evaluation of the dynamic model of fluidic muscles using quick-release," in *Proc. 1st IEEE/RAS-EMBS Int. Conf. Biomed. Robot. Biomechatron.*, Pisa, Italy, Feb. 2006, pp. 637–642.

[18] P. B. Petrovic, "Modeling and control of an artificial muscle part one: Model building," in *Proc. X-th Conf. Mechan. Vibrations*, Temisoara, Romania, May 2002, pp. 93–98.

[19] C. P. Chou and B. Hannaford, "Measurement and modeling of McKibben pneumatic artificial muscles," *IEEE Trans. Robot. Autom.*, vol. 12, no. 1, pp. 90–102, Feb. 1996.

[20] N. Tsagarakis and D. G. Caldwell, "Improved modelling and assessment of pneumatic muscle actuators," in *Proc. IEEE Int. Conf. Robot. Autom.*, San Francisco, CA, Apr. 2000, pp. 3641–3646.

[21] D. B. Reynolds, D. W. Repperger, C. A. Phillips, and G. Bandry, "Modeling the dynamic characteristics of pneumatic muscle," *Annals Biomed. Eng.*, vol. 31, no. 3, pp. 310–317, Mar. 2003.

[22] J. E. Slotine and W. Li, *Applied Nonlinear Control*. Beijing, China: China Machine Press, 2004.

[23] B. Yao and R. G. Dontha, "Integrated direct/indirect adaptive robust precision control of linear motor drive systems with accurate parameter estimations," in *Proc. 2nd IFAC Conf. Mechatron. Syst.*, Berkeley, CA, Dec. 2002, pp. 633–638.

[24] B. Yao, "Adaptive robust control: theory and applications to integrated design of intelligent and precision mechatronic systems," in *Proc. Int. Conf. Intell. Mechatron. Autom.*, Chengdu, China, Aug. 2004, pp. 35–40.

[25] K. J. Astrom and B. Wittenmark, *Adaptive Control (2nd Edition)*. Boston, MA: Addison-Wesley, 1995.

[26] B. Yao, F. P. Bu, J. Reedy, and G. T. C. Chiu, "Adaptive robust motion control of single-rod hydraulic actuators: theory and experiments," *IEEE/ASME Trans. Mechatron.*, vol. 5, no. 1, pp. 79–91, Mar. 2000.

[27] B. Yao and M. Tomizuka, "Adaptive robust control of SISO nonlinear systems in a semi-strict feedback form," *Automatica*, vol. 33, no. 5, pp. 893–900, May 1997.

[28] H. K. Khalil, *Nonlinear Systems,(2nd Edition)*. Englewood Cliffs, NJ: Prentice-Hall, 1996.

[29] Fluidic Muscle DMSP/MAS. MAS_EN.pdf [Online]. Available: http://catalog.festo.com/data/CAT_PDF/001/

[30] L. Xu and B. Yao, "Adaptive robust precision motion control of linear motors with negligible electrical dynamics: theory and experiments," *IEEE/ASME Trans. Mechatron.*, vol. 6, no. 4, pp. 444–452, Dec. 2001.

Xiaocong Zhu received the Ph.D. degree and B.Eng. degree in mechanical engineering from the Zhejiang University, Hangzhou China, in 2007 and 2002, respectively.

She is currently a Postdoctor in the State Key Laboratory of Fluid Power Transmission and Control, Zhejiang University, Hangzhou, China. Her research interests include pneumatic servo control, nonlinear control theory and applications, mechatronic control, etc.

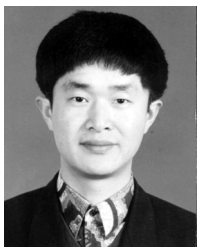

Guoliang Tao received the Ph.D. degree, M.Eng. degree and B. Eng. degree in mechanical engineering from the Zhejiang University, Hangzhou China, in 2000, 1991 and 1985, respectively.

Since 1991, he has been with State Key Laboratory of Fluid Power Transmission and Control, Zhejiang University, Hangzhou, China and was promoted to an Associate Researcher in 1997 and a Professor in 2001. His research interests include nonlinear control theory and applications, mechatronic control, fluid power transmission and control, especially pneumatic servo control, novel pneumatic components.

Bin Yao (M'96) received the Ph.D. degree in mechanical engineering from the University of California, Berkeley, USA, in 1996, the M. Eng. degree in electrical engineering from the Nanyang Technological University, Singapore, in 1992, and the B.Eng. degree in applied mechanics from the Beijing University of Aeronautics and Astronautics, Beijing, China, in 1987.

Since 1996, he has been with the School of Mechanical Engineering, Purdue University, Lafayette, USA, and was promoted to an Associate Professor in 2002 and a Full Professor in 2007. He is one of the Kuang-piu Professors with the Zhejiang University, China. His research interests include the design and control of intelligent high performance coordinated control of electromechanical/hydraulic systems, optimal adaptive and robust control, nonlinear observer design and neural networks for virtual sensing, modeling, fault detection, diagnostics, and adaptive fault-tolerant control, and data fusion. He has been actively involved in various technical professional societies such as ASME and IEEE.

Jian Cao received the B. Eng. degree in fluid power transmission and control from the Inner Mongolia University of Science & Technology, Baotou, China, in 2002.

He is currently a candidate for Ph.D. in the State Key Laboratory of Fluid Power Transmission and Control, Zhejiang University, Hangzhou, China. His research interests include fluid power transmission and control, mechatronic control, etc.